1521-009X/48/4/288–296$35.00
DRUG METABOLISM AND DISPOSITION

https://doi.org/10.1124/dmd.119.089599
Drug Metab Dispos 48:288–296, April 2020

Critical Impact of Drug-Drug Interactions via Intestinal CYP3A in the Risk Assessment of Weak Perpetrators Using Physiologically Based Pharmacokinetic Models[S]

Makiko Yamada, Shin-ichi Inoue, Daisuke Sugiyama, Yumi Nishiya, Tomoko Ishizuka, Akiko Watanabe, Kengo Watanabe, Shinji Yamashita, and Nobuaki Watanabe

Drug Metabolism and Pharmacokinetics Research Laboratories, Daiichi Sankyo Co., Ltd., Tokyo, Japan (M.Y., S.I., D.S., Y.N., T.I., A.W., K.W., N.W.) and Faculty of Pharmaceutical Sciences, Setsunan University, Osaka, Japan (S.Y.)

Received October 11, 2019; accepted January 18, 2020

ABSTRACT

A great deal of effort has been being made to improve the accuracy of the prediction of drug-drug interactions (DDIs). In this study, we addressed CYP3A-mediated weak DDIs, in which a relatively high false prediction rate was pointed out. We selected 17 orally administered drugs that have been reported to alter area under the curve (AUC) of midazolam, a typical CYP3A substrate, 0.84–1.47 times. For weak CYP3A perpetrators, the predicted AUC ratio mainly depends on intestinal DDIs rather than hepatic DDIs because the drug concentration in the enterocytes is higher. Thus, DDI prediction using simulated concentration-time profiles in each segment of the digestive tract was made by physiologically based pharmacokinetic (PBPK) modeling software GastroPlus. Although mechanistic static models tend to overestimate the risk to ensure the safety of patients, some underestimation is reported about PBPK modeling. Our in vitro studies revealed that 16 out of 17 tested drugs exhibited time-dependent inhibition (TDI) of CYP3A, and the subsequent DDI simulation that ignored these TDIs provided false-negative results. This is considered to be the cause of past underestimation. Inclusion of the DDI parameters of all the known DDI mechanisms, reversible inhibition, TDI, and induction, which have opposite effects on midazolam AUC, to PBPK model was successful in improving predictability of the DDI without increasing false-negative prediction as trade-off. This comprehensive model-based analysis suggests the importance of the intestine in assessing weak DDIs via CYP3A and the usefulness of PBPK in predicting intestinal DDIs.

SIGNIFICANCE STATEMENT

Although drug-drug interaction (DDI) prediction has been extensively performed previously, the accuracy of prediction for weak interactions via CYP3A has not been thoroughly investigated. In this study, we simulate DDIs considering drug concentration-time profile in the enterocytes and discuss the importance and the predictability of intestinal DDIs about weak CYP3A perpetrators.

Introduction

When the potential for drug-drug interactions (DDIs) is suggested by the results of in vitro studies during the development of a new drug, the magnitude of the in vivo DDIs is predicted using models, such as static models or physiologically based pharmacokinetic (PBPK) models, to determine the necessity of clinical studies (Food and Drug Administration, 2017). In general, an area under the curve ratio (AUCR) of a substrate with or without a perpetrator between 0.8 and 1.25 represents no DDIs. Many previous studies have focused on predicting strong interactions; however, it is important to predict weak interactions around the thresholds accurately because they influence strategies for drug development. Because the risk in clinical DDI studies is low but not zero for participants and the cost burden to the drug development process is passed on to the healthcare system, unnecessary studies should be avoided (Greenblatt, 2014). In our survey using PharmaPendium (Elsevier, Amsterdam, Netherlands), a data base of drug approval documents, among the compounds for which product labels include the results of clinical DDI studies with midazolam, approximately half of the labels stated that there was no interaction (Supplemental Data). These studies may not have been needed if the interaction could have been accurately predicted. Although a static model is useful to evaluate DDI risk, it assumes that theoretical maximum concentrations are sustained, which is not true in the in vivo environment and often leads to a false-positive prediction. Vieira et al. (2014) evaluated the predictability of a mechanistic static model using 119 clinical DDI study results with midazolam, a typical CYP3A substrate, and although the false-negative

https://doi.org/10.1124/dmd.119.089599.
[S]This article has supplemental material available at dmd.aspetjournals.org.

ABBREVIATIONS: AUC, area under the curve; AUCR, AUC ratio; $AUCR_g$, AUCR based on intestinal DDI; $AUCR_h$, AUCR based on hepatic DDI; CL, systemic clearance; C_{ss}, steady-state plasma concentration; DDI, drug-drug interaction EC_{50} half maximum effective concentration; E_{max}, maximum induction effect; F_a, fraction absorbed; F_g, intestinal availability; FPE, first-pass effect; f_m, fraction of CL of a substrate mediated by the enzyme that is subject to inhibition/induction; $f_{u,inc}$, in vitro unbound fraction $f_{u,p}$ unbound fraction in plasma; $[I]_g$, concentration of perpetrator in intestine for static model; K_{12}, rate constant for the distribution of the drug to the second compartment; K_{21}, rate constant for the distribution of the drug from the second compartment; k_a, first-order absorption rate constant; K_i, reversible inhibition; K_I, concentration at half k_{inact}; k_{inact}, inactivation rate constant; K_m, Michaelis-Menten constant; k_{obs}, apparent inactivation rate constant; NADPHgs, NADPH Regeneration System; PBPK, physiologically based PK; PK, pharmokinetic; TDI, time-dependent inhibition; V_c, central compartment volume; V_{max}, maximum value of metabolic activity.

rate was low (2.3%), the false-positive rate was approximately 70%. A recent systematic study by Hsueh et al. (2018) concluded that PBPK models are useful in the determination of the necessity of clinical trials; however, the negative predictive error was approximately 50%. Although most false-negative cases involve weak inhibitors, their underestimation is undesirable.

For the prediction of weak interactions, the presence or absence of interaction often depends on intestinal interactions because the drug concentration in enterocytes is usually higher than in hepatocytes. To predict intestinal DDI more accurately, it is necessary to create a PBPK model that simulates an enterocyte concentration-time profile based on the behavior of a compound during absorption. When predicting the DDI of strong inhibitors, CYP3A in the intestine is maximally inhibited; therefore, the reciprocal of intestinal availability (F_g), $1/F_g$, can be used as the magnitude of the DDI in the intestine (Galetin et al., 2007, 2008). Various studies focused on the predictability of strong DDIs, thus the accuracy of prediction for intestinal interactions has not been as thoroughly investigated as that for hepatic interactions.

Another important point is the use of appropriate in vitro DDI parameters. When we individually examined the models that exhibited false-negative predictions in past studies (Hsueh et al., 2018), we discovered that only inhibition constants for reversible inhibition (K_i) were calculated for some perpetrators, even though the potential of time-dependent inhibition (TDI) and induction was suggested in other studies (Zimmerlin et al., 2011; Vieira et al., 2014). For compounds that exhibit both reversible inhibition and TDI, ignoring TDI parameters may cause underestimation. In addition, the evaluation of the predictability of DDIs for compounds that exhibit both inhibition and induction is insufficient. Because of this, the DDI guidance recommends a conservative approach in which the inhibition and induction mechanisms are considered separately (Food and Drug Administration, 2017), and this leads to overestimation of the DDI risk.

In this study, calculations were conducted using virtual compounds with various CYP3A inhibitory activities by static models to show the importance of the intestine in DDI prediction. Subsequently, reversible inhibition, TDI, and the induction potential of CYP3A were evaluated by in vitro experiments to obtain data under identical conditions for weak perpetrators, wherein observed midazolam AUCR in a clinical DDI study was less than 2. The effects of reversible inhibition, TDI, and induction were simulated separately and concurrently by PBPK models using the DDI module in GastroPlus (ver. 9.6.0001; Simulation Plus, Lancaster, CA), which incorporated the Advanced Compartmental Absorption and Transit model enabling a physiologically relevant simulation of the concentration-time profiles in each segment of the digestive tract, and the accuracy of the prediction was evaluated.

Materials and Methods

Compounds and Reagents

Midazolam was purchased from Wako Pure Chemical Industries (Osaka, Japan). The metabolite of midazolam, 1′-hydroxymidazolam, was purchased from Sigma-Aldrich (St. Louis, MO). As an internal standard, ^{13}C-1′-hydroxymidazolam was obtained from Corning (Corning, NY). The following marketed drugs were used for the evaluation of the potential to inhibit or induce CYP3A: atomoxetine hydrochloride (Tokyo Chemical Industry, Tokyo, Japan), atorvastatin (LKT Laboratories, St. Paul, MN), azithromycin dehydrate (LKT Laboratories), casopitant mesylate (Santa Cruz Biotechnology, Dallas, TX), cimetidine (Sigma-Aldrich), deferasirox (Toronto Research Chemicals, North York, Canada), ethinyl estradiol (Sigma-Aldrich), everolimus (Selleck Chemicals, Houston, TX), felodipine (Sigma-Aldrich), fluoxetine (Sigma-Aldrich), fluvoxamine (Sigma-Aldrich), pazopanib (ChemieTek, Indianapolis, IN), ranitidine hydrochloride (Sigma-Aldrich), roxithromycin (Sigma-Aldrich), simvastatin (Wako Pure Chemical), suvorexant (AdooQ-BioScience, Irvine, CA), and tadalafil (Selleck Chemicals). Pooled human microsomes (mixed sex, 20 mg protein/ml) and pooled cryopreserved human hepatocytes were purchased from Sekisui XenoTech, LLC (Kansas City, KS). NADPH Regeneration System Solution A and NADPH Regeneration System Solution B were purchased from Corning.

Clinical DDI Study Data Collection

The AUCR values for midazolam in the presence of CYP3A perpetrators in clinical DDI studies were collected from the Drug Interaction Database (https://www.druginteractioninfo.org/, University of Washington, Seattle, WA); in vitro DDI data were also collected from the Drug Interaction Database. Seventeen marketed drugs were chosen for the current study, in which the AUCR of midazolam was 0.8–2 in the clinical DDI study, and an inhibitory effect on CYP3A was observed in the in vitro study. A summary of the clinical studies used in the prediction is shown in Supplemental Table 1.

Determination of In Vitro Perpetrator Parameters for CYP3A

Inhibition. The potential for reversible and time-dependent inhibition of the 17 marketed drugs (atomoxetine, azithromycin, atorvastatin, casopitant, cimetidine, deferasirox, ethinyl estradiol, everolimus, felodipine, fluoxetine, fluvoxamine, pazopanib, ranitidine, roxithromycin, simvastatin, suvorexant, and tadalafil) on CYP3A was investigated using pooled human liver microsomes. To reduce the effect of protein binding to microsomal proteins, relatively low protein concentrations (0.02 mg/ml for reversible inhibition and 0.2 mg/ml for TDI) were used. The activity of CYP3A was estimated from the assay of midazolam 1′-hydroxylation activity. The perpetrators were dissolved in acetonitrile or methanol, and midazolam was dissolved in methanol:water [1:1]; the final concentration of the solvent was less than 1.5%. Methanol and acetonitrile were chosen as the solvent instead of DMSO, which is frequently used to dissolve lipophilic compounds, because DMSO affects the TDI activity of some compounds, most likely via the inhibition of metabolism (Nishiya et al., 2010; Aasa et al., 2013). For reversible inhibition, the incubation mixtures containing human liver microsomes, potassium phosphate buffer, midazolam (2, 4, and 8 μM), and each perpetrator were prewarmed at 37°C for 5 minutes. Then incubation was initiated by the addition of the final concentrations of 5% for the NADPH Regeneration System Solution A and 1% for the NADPH Regeneration System Solution B (NADPHgs). After incubation at 37°C for 5 minutes, the reaction was terminated by mixing with a stop solution [acetonitrile:methanol (1:1) containing an internal standard]. To determine the inactivation parameters for TDI, the incubation mixture without midazolam was prewarmed at 37°C for 5 minutes, and the NADPHgs were added to initiate the incubation. Samples were taken immediately (at 0 minutes) and, at 15, 30, and 60 minutes after the start of incubation, diluted ten times with the incubation mixture containing NADPHgs and midazolam (40 μM), and then they were incubated for 5 minutes; subsequently, the reaction was terminated by mixing with the stop solution. The samples were centrifuged, and the concentrations of the midazolam metabolite, 1′-hydroxymidazolam, in each supernatant was measured using liquid chromatography-tandem mass spectrometry. More details of the method are shown in the Supplemental Method.

The metabolic activity (picomoles per minute per milligram protein) of CYP3A was obtained by dividing the 1′-hydroxymidazolam concentration by microsomal protein concentration and incubation time and analyzed by eqs. 1–3 using Phoenix WinNonlin Ver. 6.3 (Certara, Princeton, NJ).

$$\text{Competitive inhibition}: \ E = V_{max} \times S/(K_m(1 + I/K_i) + S) \quad (1)$$

$$\text{Noncompetitive inhibition}: \ E = V_{max} \times S/((K_m + S) \times (1 + I/K_i)) \quad (2)$$

$$\text{Uncompetitive inhibition}: \ E = V_{max} \times S/(K_m + S(1 + I/K_i)) \quad (3)$$

where E is the metabolic activity, V_{max} is the maximum value of metabolic activity, S is the substrate concentration, K_m is the Michaelis constant, and I is the concentration of the test compound. After consideration of Akaike's information criterion, the most appropriate model was selected to determine K_i.

To calculate the inactivation parameters, the natural logarithm of the remaining activity at each drug concentration was plotted against the preincubation time. The apparent inactivation rate constant (k_{obs}) was determined from the negative slope of the fitting line from the area showing an initial inhibition rate for each drug concentration. To determine the maximum inactivation rate constant (k_{inact}) and the concentration at half k_{inact} (K_I) of the drug, the relationship between the k_{obs}

value and I was fitted into the eq. 4 using WinNonlin. When a decrease in k_{obs} was observed at higher concentrations, the data were removed, and the parameters were calculated using the remaining data.

$$k_{obs} = k_{inact} \times I/(K_I + I) \quad (4).$$

Induction. The potential of 13 marketed drugs (azithromycin, atomoxetine, cimetidine, casopitant, deferasirox, everolimus, felodipine, fluvoxamine, pazopanib, ranitidine, roxithromycin simvastatin, and tadalafil) to induce CYP3A4 was investigated using pooled cryopreserved human hepatocytes. For the remaining four compounds (atorvastatin, ethinyl estradiol, fluoxetine, and suvorexant), the values from the literature were available. Rifampicin (10 μM) and omeprazole (50 μM) were used as positive controls, and gatifloxacin (10 μM) was used as a negative control. The drugs were dissolved in DMSO and diluted 1000 times in modified Lanford medium (Nissui Pharmaceutical, Tokyo, Japan). The hepatocytes were seeded at 6×10^4 cells/well in 96-well culture plates and left to adhere overnight. On the day after, the incubation medium was replaced with the medium containing drugs, and the plate was cultured overnight. These steps were repeated, resulting in a total treatment time of 48 hours. All experiments were performed in triplicate. After the incubation, the RNA was extracted and analyzed by reverse transcription-polymerase chain reaction. Relative mRNA expression was calculated by dividing the quantity of CYP3A4 mRNA by the quantity of glyceraldehyde-3-phosphate dehydrogenase mRNA. A more detailed method is shown in the Supplemental Method.

The fold change in expression was calculated by dividing the mRNA expression of the drug by the mRNA expression of the same gene in the solvent-treated control sample. The induction parameters, the maximum induction effect (E_{max}) and half maximum effective concentration (EC_{50}), were calculated using eq. 5 using Phoenix WinNonlin (ver. 6.3).

$$\text{Fold induction} = 1 + E_{max} \times I/(EC_{50} + I) \quad (5).$$

Prediction Using Mechanistic Static Model

The AUCR of midazolam with and without the perpetrator was predicted using a mechanistic static model with eq. 6, in accordance with the draft guidance for DDI by the Food and Drug Administration (Food and Drug Administration, 2017).

$$AUCR = [1/[(A_g \times B_g \times C_g) \times (1–F_g) + F_g]] \times [1/[(A_h \times B_h \times C_h) \times f_m + (1–f_m)]] \quad (6).$$

In eq. 6, F_g is the fraction available after intestinal metabolism, and f_m is the fraction of systemic clearance (CL) of a substrate mediated by the enzyme that is subject to inhibition/induction; subscripts "h" and "g" denote the liver and gut, respectively. The F_g of midazolam was calculated to be 0.54 based on the absolute bioavailability (0.30) and hepatic availability (0.56) from literature (Thummel et al., 1996), assuming the fraction absorbed (F_a) was 1. The f_m of midazolam was set to 0.93 (Zhou and Zhou, 2009). Although F_g and f_m change depending on the dose of midazolam, constant values were used for the static model analysis. Terms A, B, and C represent reversible inhibition, TDI, and induction, respectively, and were calculated from the following eqs. 7–9:

$$A = \frac{1}{1 + \frac{[I]}{K_i}} \quad (7)$$

$$B = \frac{k_{deg}}{k_{deg} + \frac{[I] \times k_{inact}}{[I] + K_I}} \quad (8)$$

$$C = 1 + \frac{d \cdot E_{max} \cdot [I]}{[I] + EC_{50}} \quad (9)$$

where k_{deg} is the apparent first-order degradation rate constant of CYP3A, and 0.0005 minute^{-1} was used both for gut and liver (Zhang et al., 2009), which is the same value used in GastroPlus ver. 9.6.0001; d is calibration factor, and 1 was used.

To calculate the concentration of perpetrator in intestine ($[I]_g$), eq. 10 (Rostami-Hodjegan and Tucker, 2004) was used as recommended in the DDI guidance by the Food and Drug Administration.

$$[I]_g = F_a \times k_a \times \text{Dose}/Q_{en} \quad (10)$$

where k_a is the first-order absorption rate constant, and Q_{en} is the blood flow through enterocytes (18 L/h) (Yang et al., 2007).

When the DDI of the marketed drugs was predicted, F_a used in the static model was the same as that calculated by GastroPlus (Supplemental Table 3) to allow comparison with the result of the analysis. Because GastroPlus calculates time-dependent k_a instead of single k_a, the k_a for the static model analysis was calculated from the concentration-time profile of each drug from the literature using Phoenix WinNonlin (Supplemental Table 3). The unbound fraction in plasma ($f_{u,p}$) was adjusted by GastroPlus for possible binding to plasma lipids ($f_{u,p,adj}$, Supplemental Table 4). For the calculation of steady-state plasma concentration (C_{ss}), AUC_{inf} at a single dose was simulated with GastroPlus and used. Most of the in vitro DDI parameters used were obtained in the current study; the induction data of atorvastatin (Vieira et al., 2014), ethinyl estradiol (Fahmi et al., 2008), fluoxetine (Fahmi et al., 2008), and suvorexant (Prueksaritanont et al., 2013) were obtained from the literature. K_i, K_I, and EC_{50} were corrected to the unbound value using the in vitro unbound fraction ($f_{u,inc}$), predicted by GastroPlus (Supplemental Table 4). When $f_{u,inc}$ was calculated for the microsomes and hepatocytes, Calc (Hallifax)-HLM (Hallifax and Houston, 2006) and Calc (Austin)-Hep (Austin et al., 2005) in GastroPlus were used, respectively.

Static Model Analysis of Virtual Compounds

To show the importance of the interaction in the intestine, the AUCR of virtual compounds with various K_i values (from 0.2 to 100 μM) was calculated using a mechanistic static model. The properties of the virtual compound were as follows: mol. wt., 500; F_a, 1; k_a, 1 hour^{-1}; CL, 20 L/h; and $f_{u,p}$, 0.1. For the concentration of the perpetrator in the liver ($[I]_h$), the unbound C_{ss} was calculated by dividing the AUC by dosing interval, and AUC was calculated by dividing the dose by CL. The AUCR based on CYP3A inhibition in the intestine, liver, and both the intestine and liver were calculated at a daily dose of 100 mg. In addition, the AUCR was calculated with fixed K_i (1 μM) and various doses (1–500 mg).

Prediction Using PBPK Model

GastroPlus version 9.6.0001 was used to construct the human PBPK model. The Advanced Compartmental Absorption and Transit model, compartmental PK model, and DDI module in GastroPlus were used to simulate intestinal absorption and metabolism, systemic distribution and elimination, and DDI, respectively. For parameters that are not specifically described below, the values incorporated into, or predicted by, GastroPlus were used (e.g., human physiologic parameters).

Substrate (Midazolam) Model. The parameters used for the midazolam model are shown in Table 1. The effective permeability (P_{eff}), octanol-water partition coefficient (logP), blood-to-plasma concentration ratio, $f_{u,p}$, and solubility data were obtained from the literature (Andersin, 1991; Gertz et al., 2011). The $f_{u,p}$ was adjusted by GastroPlus for possible binding to plasma lipids. The distribution parameters, the central compartment volume (V_c), rate constant for the distribution of the drug to the second compartment (K_{12}), and rate constant for the distribution of the drug from the second compartment (K_{21}), were determined using the PKPlus module in GastroPlus to fit the plasma concentration-time profile after intravenous and oral administration of midazolam (Thummel et al., 1996). The in vitro kinetic parameters of midazolam metabolism by CYP3A [i.e., K_m and V_{max}] were obtained from literature (Thummel et al., 1996), and then V_{max} was converted to in vivo values using microsomal protein concentration (38 mg/g liver) and liver weight (1800 g), the default values in GastroPlus ver. 9.6. To predict intestinal metabolism, GastroPlus uses the enzyme-kinetic parameters generated from human liver microsomes based on the abundance ratio of the enzyme (Agoram et al., 2001). The intrinsic clearance values obtained from human liver microsomes and human intestinal microsomes are not significantly different after normalization for tissue-specific CYP3A abundance (Gertz et al., 2010), and the prediction error of F_g by GastroPlus is less than 2-fold (Heikkinen et al., 2012). In the current study, about 2-fold underestimation of midazolam F_g was observed when the same V_{max} for liver and intestine was used; therefore, the V_{max} for intestinal CYP3A was reduced by approximately half to achieve the observed F_g (0.54). The use of a different V_{max} for the liver and intestine was not originally intended, but it was essential to improve the accuracy of the prediction.

Perpetrator Model. The solubility, P_{eff}, logP, and $f_{u,p}$ of the 17 marketed drugs were collected to construct the perpetrator models (Supplemental Tables 4–6). These data were collected from data bases (PubChem, https://pubchem.ncbi.nlm.nih.gov/; and the Drug Interaction Database, https://www.druginteractioninfo.org/, University of Washington), determined in in-house studies, obtained from literature, or predicted from the compound structure by the ADMET Predictor incorporated in GastroPlus. When the solubility in water was known, and the pH of the aqueous solution was unknown, the pH of the saturated solution was predicted using GastroPlus. The bile salt influence on in vivo solubility (solubilization ratio) was calculated from the biorelevant solubility predicted by GastroPlus (Supplemental Table 5). The solubility versus pH profiles were calculated from the solubility at reference pH and pK_a (Supplemental Table 5) by GastroPlus. For seven drugs, the predicted dissolution rate did not appear to be appropriate, thus the particle size was decreased from the default radius of 25 μm to fit the observed concentration-time profile. Although it may be necessary to change the precipitation time in some cases, the default value (900 seconds) was used for all compounds in this study. The PK parameters, such as CL, V_c, K_{12}, and K_{21}, were optimized to fit the concentration-time profiles after oral administration obtained from literature (Supplemental Table 7). Although it is desirable to fit the profiles after intravenous administration, they were unavailable for most compounds. For compounds with known large first-pass effects (FPEs), FPE was calculated and input into GastroPlus models using bioavailability, CL (assumed to be equal to hepatic clearance), F_g, and hepatic blood flow, obtained from the literature and from a data base, assuming that F_a was 1. The calculated FPE is shown in Supplemental Table 7. For the gut physiology model, "Human-Physiological-Fasted" or "Human-Physiological-Fed," as incorporated in the software, was used depending on the food condition of the source clinical studies. The absorption scaling factor was calculated by Opt logD Model SA/V 6.1 incorporated in the software. The unbound fraction in enterocytes was set to 100% (default value).

DDI Simulation. DDI simulation for midazolam and each perpetrator was conducted using the dynamic simulation in the DDI module of GastroPlus. The dosing information of substrate and perpetrators is summarized in Supplemental Table 1. The simulation used four different settings: 1) reversible inhibition parameter only, 2) both reversible inhibition and TDI parameters, 3) induction parameter only, and 4) all parameters available, to compare the effect of each mechanism. The AUCRs based on the interactions in the gut and liver were calculated separately [AUCR based on intestinal DDI ($AUCR_g$) and AUCR based on hepatic DDI ($AUCR_h$), respectively].

Evaluation of Predictive Performance

The traditional approach to evaluate the predictive performance based on whether predictions fall within a 2-fold range of the observed data is not suitable for weak perpetrators. For example, when actual AUC ratio is 1.5 (weak inhibitor), the acceptance range is from 0.75 (inducer) to 3 (moderate inhibitor). Therefore, the success rate of the prediction was calculated using the method proposed by Guest et al. (2011) using eqs. 11–13.

$$\text{Upper limit} = R_{obs} \times \text{Limit} \tag{11}$$

$$\text{Lower limit} = R_{obs}/\text{Limit} \tag{12}$$

TABLE 1

Physicochemical and pharmacokinetic parameters of midazolam used for simulation

Parameters (U)			
Mol. wt.	325.77	V_c (L/kg)	0.326
logP	3.25[a]	K_{12} (1/h)	1.57
$f_{u,p}$ (%)	3.1[a] (2.32[b])	K_{21} (1/h)	1.05
Blood/plasma conc. ratio	0.55[a]	V_2 (L/kg)	0.489
P_{eff} (cm/s × 10^{-4})	6.73[a]	CYP3A_K_m (μg/ml)	0.896[c]
Solubility (mg/ml)	0.082[d]	CYP3A_$V_{max,\ liver}$ (mg/s)	0.373[c]
		CYP3A_$V_{max,\ gut}$ (mg/s)	0.184[e]

[a]Gertz et al. 2011.
[b]The value was adjusted by GastroPlus for possible binding to plasma lipids.
[c]Thummel et al. (1996), the values were converted using the unit converter in GastroPlus.
[d]Andersin (1991), pH 6.39.
[e]V_{max} for intestinal CYP3A was adjusted to achieve the observed F_g (0.54).

$$\text{Limit} = \frac{\delta + 2(R_{obs} - 1)}{R_{obs}} \tag{13}$$

where R_{obs} is observed AUCR or reciprocal of observed AUCR for inhibitor (AUCR > 1) or inducer (AUCR < 1), respectively, and δ is a parameter that accounts for variability. When δ = 1, there is no variability, and when δ = 1.25 (used in this study) and R_{obs} = 1, then the limits on AUCR are between 0.80 and 1.25, corresponding to the conventional 20% limits used in bioequivalence testing.

Results

Static Model Analysis of Virtual Compounds. To show the contribution of liver and intestine, the AUCR of midazolam was calculated by static models with K_i value ranging from 0.2 to 100 μM and fixed-dose (100 mg) or a fixed K_i (1 μM) and dose ranging from 1 to 500 mg. The results are shown in Fig. 1, respectively. According to the properties of the virtual compounds written in the method, the $[I]_g$ and $[I]_h$ of the virtual compounds were 11.1 and 0.416 μM at 100 mg of dose, respectively. When the inhibition was weak (i.e., K_i was large, or dose was small), the AUCR caused by the interaction in the intestine was larger than that in the liver. When the inhibition is strong, the DDI in the intestine is saturated to $1/F_g$ (AUCR: 1.85), and the effect in the liver is larger.

In Vitro DDI Study. The parameters for reversible inhibition and TDI are summarized in Table 2, and the kinetic plots are shown in Supplemental Figs. 1 and 2, respectively. Among the 17 tested marketed drugs (atomoxetine, azithromycin, atorvastatin, casopitant, cimetidine, deferasirox, ethinyl estradiol, everolimus, felodipine, fluoxetine, fluvoxamine, pazopanib, ranitidine, roxithromycin, simvastatin, suvorexant, and tadalafil), 16 drugs (all drugs except azithromycin) showed reversible inhibition, and K_i was calculated (Table 2). The reversible inhibition of azithromycin was very weak, and K_i was above the maximum concentration of the inhibitor tested (>1000 μM). Ethinyl estradiol and tadalafil were considered to be noncompetitive inhibitors by the analysis of Akaike's information criterion, and the other 14 drugs were considered to be competitive inhibitors. The obtained K_i values of most compounds were comparable to those already reported in the literature (Supplemental Table 2). Among the 17 tested marketed drugs, 16 drugs showed TDI, and K_I and k_{inact} were calculated (Table 2). Atomoxetine did not show TDI. When the obtained K_I and k_{inact} were compared with the values from the literature, a large difference was observed for some compounds, presumably because of the difference in the experimental conditions (Supplemental Table 2), and the difference in k_{inact}/K_I between the values in this study and from the literature was smaller than that of each K_I and $k_{inact.}$ Among the 13 marketed drugs tested for induction, seven drugs (casopitant, everolimus, felodipine, fluvoxamine, pazopanib, simvastatin, and tadalafil) had an inductive effect, and EC_{50} and E_{max} were calculated (Supplemental Fig. 3; Table 2). For the remaining six drugs (atomoxetine, azithromycin, cimetidine, deferasirox, ranitidine, and roxithromycin), the maximum fold induction was less than 2-fold. The fold induction of positive controls was 15.5–24.5 and 5.42–12.7 for rifampicin and omeprazole, respectively. No induction was observed by the negative control gatifloxacin.

DDI Prediction Using GastroPlus. DDI simulation was conducted using the dynamic simulation in the DDI module. The dosing regimens used for the simulation were the same as for the clinical studies. These are summarized in Supplemental Table 1. The plots of observed versus predicted AUCR by GastroPlus using

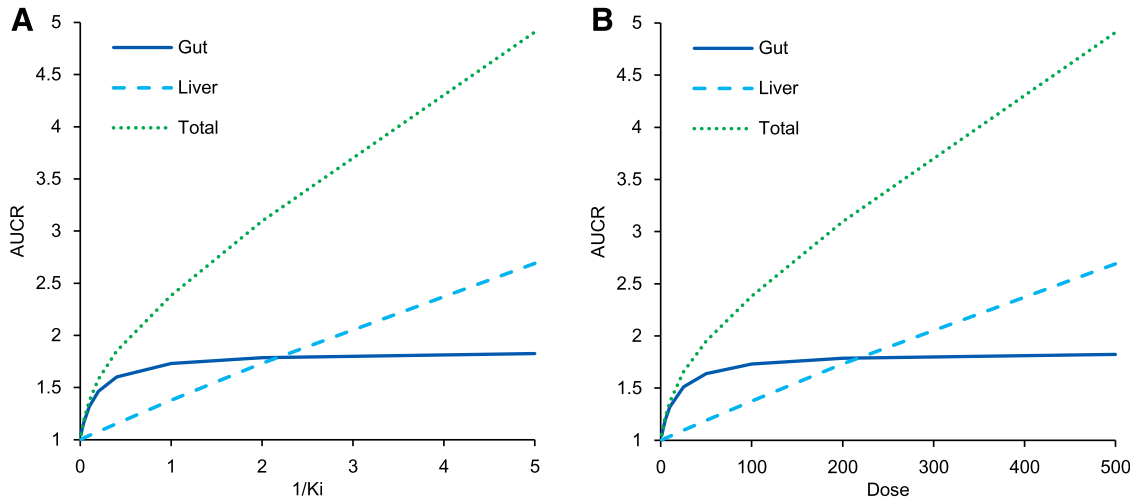

Fig. 1. The relationship between the AUCR of midazolam and K_i with fixed dose [100 mg, (A)] or doses with fixed K_i [1 μM, (B)] in static model analysis using virtual compounds.

the reversible inhibition parameter only and both reversible inhibition and TDI parameters, respectively, are shown Fig. 2. Of the seven drugs that showed positive DDIs in clinical studies, five were predicted as negative (false-negative) when only K_i was incorporated (Fig. 2A). When TDI parameters were also incorporated, all seven compounds were predicted as positive, although 4 out of the 10 compounds with observed negative DDIs were also predicted as positive; that is, they were false positives (Fig. 2B). The relationship of AUCR of midazolam observed in the clinical studies and predicted by GastroPlus with all in vitro DDI parameters (reversible inhibition, time-dependent inhibition, and induction) incorporated is shown in Table 3. The predictive performance was evaluated using the approach proposed by Guest et al. (2011) and compared with the results by static models, as shown in Fig. 3. The *y*-axis of the graphs is shown as fold error (predicted/observe). The success rate was calculated as 76% and 65% for GastroPlus and static model, respectively. An overestimation was observed in some drugs; however, there was no underestimation. The calculated $AUCR_g$ and $AUCR_h$ were also shown in Table 3. For most compounds, the $AUCR_h$ was approximately 1, and $AUCR_g$ showed a larger contribution to the change of AUCR. The relationship between $AUCR_g$ simulated by GastroPlus and the static model when inhibitory (both reversible and time-dependent) and inducing effects were simulated separately is shown in Fig. 4. For inhibition (Fig. 4A), ethinyl estradiol, ranitidine, and azithromycin showed similarly small $AUCR_g$, and pazopanib showed similarly large $AUCR_g$ in the GastroPlus and static model; everolimus and suvorexant showed larger $AUCR_g$ in GastroPlus. For other compounds, the prediction of inhibition tended to be stronger by the static model than by GastroPlus. For induction (Fig. 4B), smaller $AUCR_g$ (i.e., stronger interaction) was predicted by the static model than by GastroPlus, except for with ethinyl estradiol, for which the interaction was very weak. The relationship of predicted AUCR using inhibition, induction, and both inhibition and induction is

TABLE 2

In vitro inhibition and induction parameters used for the simulation

	Reversible Inhibition	Time-Dependent Inhibition		Induction	
Precipitant	K_i (μM)	K_I (μM)	k_{inact} (/min)	EC_{50} (μM)	E_{max}
Atomoxetine	41.6	—		—	
Atorvastatin	51.8	29.9	0.019	16.6[a]	13.5[a]
Azithromycin	—	599	0.013	—	
Casopitant	4.26	0.474	0.011	2.04	9.22
Cimetidine	202	76.8	0.0060	—	
Deferasirox	106	58.6	0.0044	—	
Ethinyl estradiol	78.1	12.3	0.053	20.0[b]	69.0[b]
Everolimus	0.647	0.675	0.016	0.00657	2.42
Felodipine	0.982	4.49	0.015	1.07	6.66
Fluoxetine	13.5	3.90	0.0015	0.50[b]	2.1[b]
Fluvoxamine	23.5	1.85	0.00087	28.0	4.42
Pazopanib	9.31	4.00	0.017	0.807	2.43
Ranitidine	847	491	0.0036	—	
Roxithromycin	43.9	0.926	0.0014	—	
Simvastatin	0.462	19.4	0.0071	5.75	43.6
Suvorexant	1.11	0.797	0.039	14.0[c]	11.0[c]
Tadalafil	32.7	4.74	0.043	1.82	21.0

—, no inhibition or induction was observed.
[a]Vieira et al. (2014).
[b]Fahmi et al. (2008).
[c]Prueksaritanont et al. (2013).

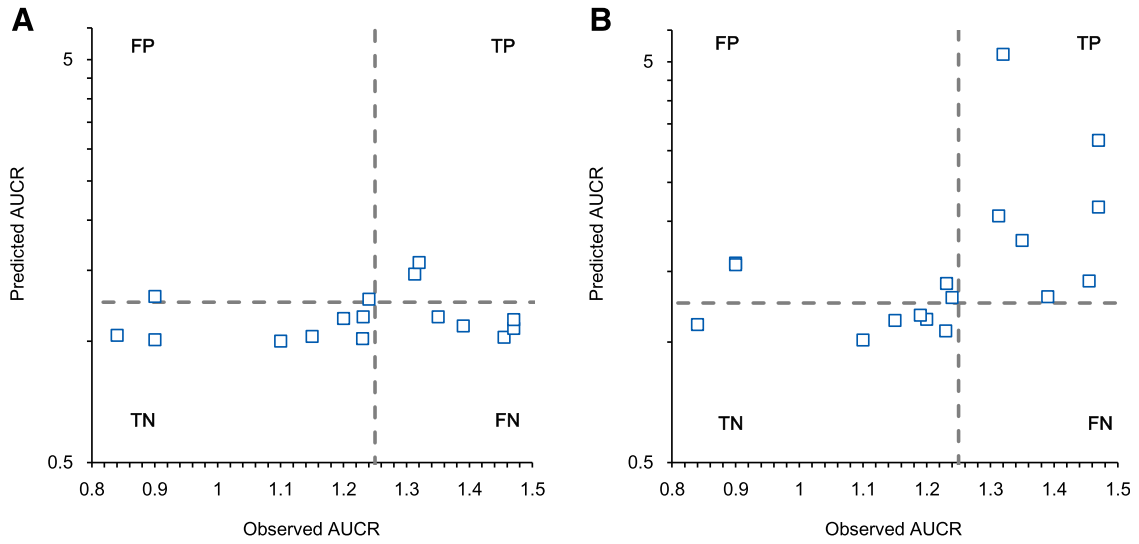

Fig. 2. Observed vs. predicted AUCR of midazolam by GastroPlus dynamic simulation using reversible inhibition only (A) and reversible and time-dependent inhibition (B). The dashed line represents 1.25-fold AUCR. FN, false negative; FP, false positive; TN, true negative; TP, true positive.

shown in Fig. 5. Incorporation of both inhibition and induction mechanisms resulted in offset; the decrease in metabolic activity due to inhibition was alleviated by the increase in enzymes due to induction.

Discussion

To judge the necessity of a clinical DDI study, the accuracy of the prediction of weak DDIs is important, and when predicting the DDI of weak inhibitors, intestinal effects are considered significant. To help imaging, the relationship between DDI in the gut and liver (Fig. 1) was prepared using virtual compounds. The left end of Fig. 1, wherein inhibition is weak, intestinal CYP3A is not completely inhibited, and liver interactions are hardly observed, suggesting the importance of intestine when discussing weak DDI. Midazolam is often used as a CYP3A probe substrate, and many clinical DDI study data are available. DDI prediction of midazolam has been extensively performed previously, but many focused on strong interactions, and to assess the predictability of DDIs via intestinal CYP3A, weak DDIs should be the focus. Therefore, 17 weak perpetrators, for which observed midazolam AUCR in a clinical DDI study was less than 2, were selected to evaluate predictability by GastroPlus. At first we tried to predict in vivo DDI using in vitro values from the literature; however, there were several problems. For some compounds, a huge variation of the parameters was observed in the literature; microsomal protein concentration, which is necessary to calculate $f_{u,inc}$, was unknown; and positive TDI or induction was reported without calculated parameters. Thus, we conducted in vitro studies to obtain the data under the same experimental conditions.

When the AUCRs of midazolam predicted by GastroPlus were compared with the observed values, the success rate was 76% by evaluation using the strict criteria for weak perpetrators proposed by Guest et al. (2011), indicating the utility of PBPK modeling approach. Only 3 out of 17 compounds clearly missed the criteria, all of which were overestimated. The absence of underestimation is very important, as models with frequent underestimation cannot be used to determine the necessity of clinical DDI studies. Among the compounds with poor

TABLE 3

Summary of predicted AUCR of midazolam by GastroPlus dynamic simulation incorporating all relevant mechanisms based on in vitro data (reversible inhibition, time-dependent inhibition, and induction as applicable)

	Observed	Predicted			Predicted/Observed
		Gut ($AUCR_g$)	Liver ($AUCR_h$)	Gut and Liver (AUCR)	
Atomoxetine	1.20	1.13	1.00	1.14	0.95
Atorvastatin	1.15	1.05	1.00	1.05	0.91
Azithromycin	1.19	1.15	1.01	1.17	0.98
Casopitant	1.46	1.24	1.01	1.25	0.86
Cimetidine	1.35	1.24	1.44	1.79	1.33
Deferasirox	0.90	1.44	1.09	1.57	1.75
Ethinyl estradiol	1.10	1.00	1.00	1.00	0.91
Everolimus	1.31	1.90	0.99	1.88	1.43
Felodipine	1.23	1.21	1.00	1.21	0.98
Fluoxetine	0.84	1.02	0.92	0.94	1.12
Fluvoxamine	1.39	1.04	1.08	1.13	0.81
Pazopanib	1.32	1.72	1.61	2.76	2.09
Ranitidine	1.23	1.05	1.01	1.07	0.87
Roxithromycin	1.47	1.18	1.84	2.17	1.48
Simvastatin	1.24	1.04	1.00	1.04	0.84
Suvorexant	1.47	1.96	1.54	3.01	2.05
Tadalafil	0.90	1.10	1.06	1.18	1.31

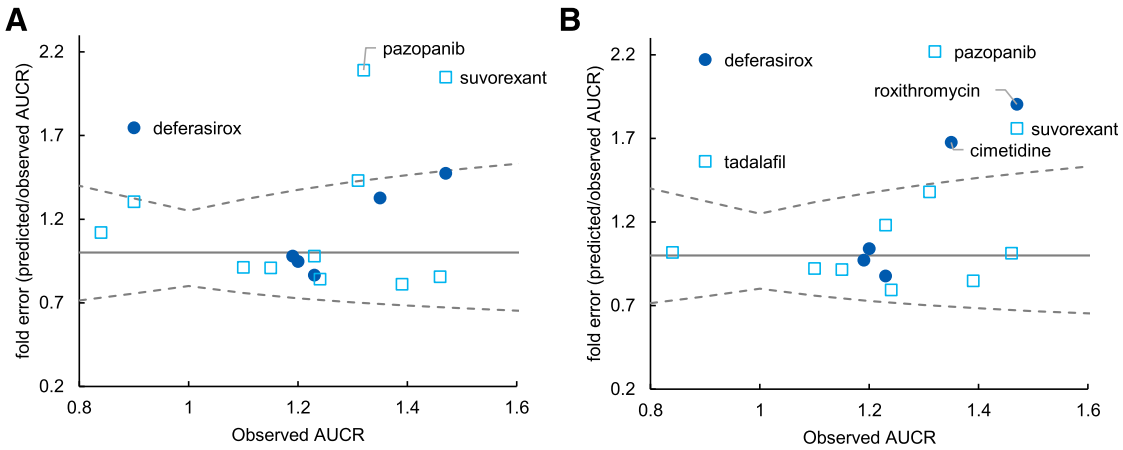

Fig. 3. Fold error of predicted midazolam AUCR via CYP3A inhibition or both inhibition and induction by GastroPlus. The closed circles represent the compounds for which only inhibitory effects were observed, and the open squares represent the compounds with both inhibition and induction in vitro. The solid line represents the line of unity, and the dashed lines represent the upper and lower limits of the success of the prediction.

predicted result, overestimation is reported about pazopanib and midazolam DDI when using TDI parameters from microsomes, and the prediction is improved by using the parameters from hepatocytes (Mao et al., 2016). The reason is not fully understood, but the involvement of plasma membranes and transporters on them has been pointed out. Thus, the cause of the overestimation in this study may be an in vitro system rather than a modeling. In addition, strong interactions of more than 2-fold and less than 0.5-fold were predicted when inhibition and induction of pazopanib were assessed separately (Fig. 5). These results may indicate the difficulty to predict the offset between strong inhibition and strong induction. Previous PBPK modeling analyses report an underestimation of weak perpetrators (Hsueh et al., 2018). However, in our study, no underestimation was observed when TDI was incorporated (Fig. 2B). Although TDIs are often considered as negative when there are no differences in IC_{50} with or without preincubation, some compounds that have been reported exhibiting no IC_{50} shifts (Haarhoff et al., 2017) showed positive TDI in our study (e.g., cimetidine, felodipine, and fluvoxamine). Sometimes preincubation results in the metabolism of the inhibitor, thereby reversible inhibition is reduced time-dependently and TDI is concealed. The absence of TDI should be determined with caution, since many compounds show the potential in screening studies (Zimmerlin et al., 2011). Thus, neglect of TDIs may contribute to the past underestimation, and it is not the problem of PBPK modeling approach itself.

Our models have some limitations. The physicochemical parameters, such as solubility, P_{eff}, and logP (or logD), have critical effects on the predicted F_a and enterocyte concentration, thus the use of experimental value is desirable. However, predicted values by ADMET Predictor were used when experimental values were not available. It is desirable to determine PK parameters after absorption, such as CL, V_c, K_{12}, and K_{21}, using plasma concentration-time profiles after intravenous administration. However, they are often unavailable in the early stages of drug development, thus we optimized the PK parameters of perpetrators (Supplemental Table 7) by fitting the data after oral administration (Supplemental Fig. 4). The efflux transporters like P-glycoprotein and breast cancer resistance protein lower the levels of the substrate in epithelial cells. Several perpetrator drugs have been reported to be substrates for these transporters; however, the facts were not included in the predictions in this study. Despite such limitations, a success rate of the predicted AUCR by GastroPlus was 76%, which suggested that this method is sufficiently useful in the prediction of the DDI risk of weak perpetrators. For some perpetrators with known large FPEs, the FPE

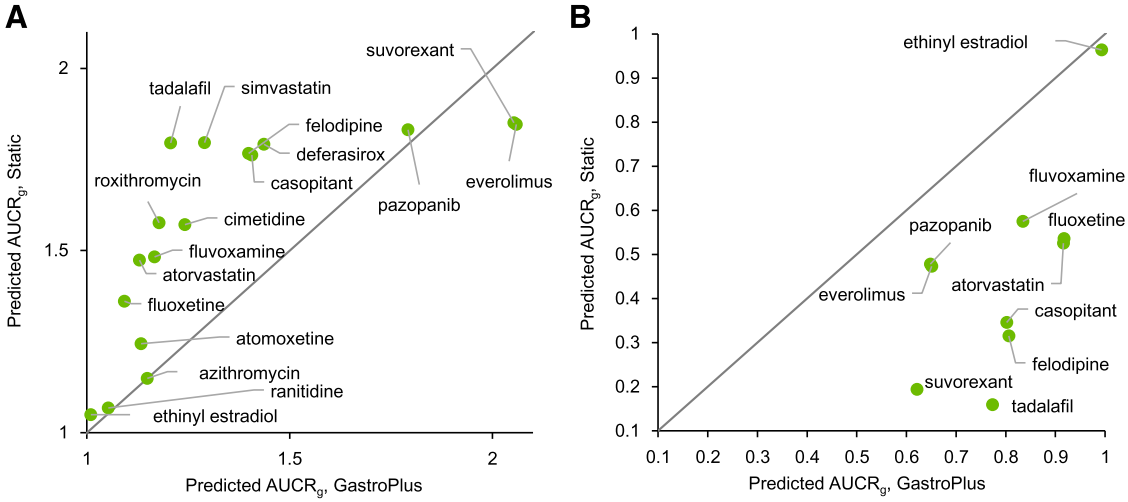

Fig. 4. The comparison of the predicted AUCR of midazolam via intestinal CYP3A inhibition (A) and induction (B) using GastroPlus and the static model. The solid line represents the line of unity.

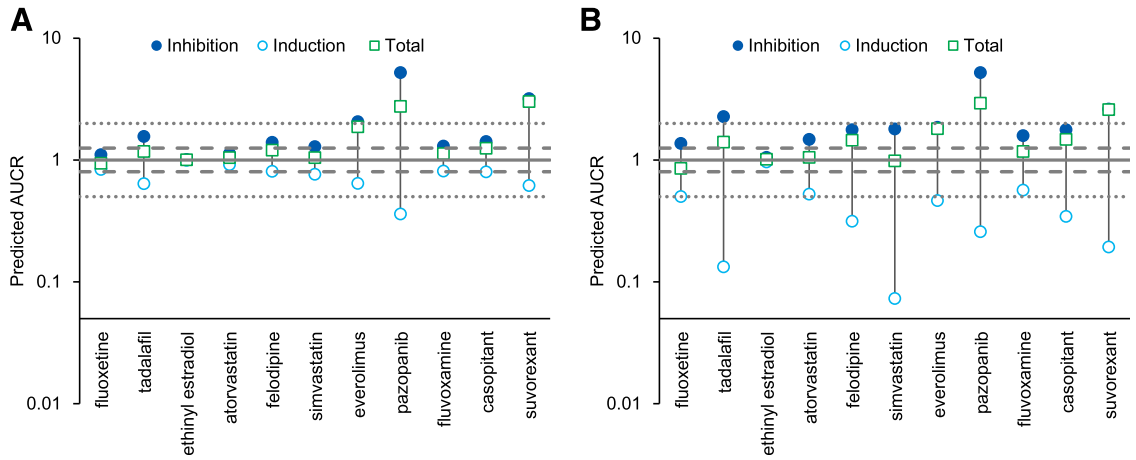

Fig. 5. The offset of inhibition and induction by GastroPlus (A) and the static model (B) for perpetrators exhibiting both inhibition and induction of CYP3A. The solid line, dashed lines, and dotted lines represent 1-, 1.25- or 0.8-, and 2- or 0.5-fold AUCR, respectively. The seven compounds from the left were compounds with no interaction in the clinical studies.

calculated from the literature PK parameters was entered. The ability to consider the metabolism of perpetrator drugs in the intestine and liver is one advantage of PBPK models over static models.

When DDIs of inhibition and induction were simulated separately, and the intestinal AUCR with GastroPlus and the static model was compared, the static models tended to predict the interaction more strongly than GastroPlus. This appeared reasonable, given that the static models assumed that the highest concentrations would persist for a long time. However, when the enterocyte concentrations calculated by GastroPlus were compared with $[I]_g$, the maximum concentration was higher than $[I]_g$, except for the compounds for which the FPE was entered. As an example, the relationship of simulated concentrations of the jejunum compartment 1 and $[I]_g$ is shown in Supplemental Fig. 5. It was suggested that the reason for the higher $AUCR_g$ was not always a higher concentration, and the duration of exposure was important. The reason for the difference in concentration is considered to be because $[I]_g$ was calculated assuming that the rates of drug influx into and efflux from epithelial cells were equal, whereas in GastroPlus influx is faster than efflux at the beginning of absorption. The difference in the F_g of midazolam is considered to be another reason for the higher $AUCR_g$ in the static models. Although F_g is constant in the static model, it is calculated by GastroPlus as small at low midazolam doses and large at high doses because GastroPlus includes saturable metabolism mechanism (Agoram et al., 2001). When simulating clinical studies with high midazolam doses (e.g., 15 mg), the AUCR was small even when the maximum inhibition of intestinal CYP3A was calculated because F_g without inhibition was close to 1. Such compounds may cause stronger interactions with lower doses of midazolam or other compounds with smaller F_g. In regard to the predictability of hepatic DDI, the correlation of $AUCR_h$ between the GastroPlus and static models was strong when an unbound C_{ss} was used for $[I]_h$ (Supplemental Fig. 6). The maximum unbound plasma concentration at the inlet to the liver, which was recommended for $[I]_h$ by DDI guidance for conservative prediction, was higher than the maximum concentration in the liver predicted by GastroPlus for most compounds (Supplemental Fig. 7). The use of unbound plasma concentration at the inlet to the liver in calculations contributed to the overestimation of static models.

When both inhibition and induction were considered simultaneously, the offset of the effects was observed (Fig. 5). The DDI guidance recommends a conservative approach in which the inhibition and induction effects are assessed separately (Food and Drug Administration, 2017) because the prediction of the offset of inhibition and induction is difficult. Although the offset of strong inhibitory and inducing effects can cause false-negative predictions, no significant underestimation was observed in our study. Therefore, when predicted inhibition and induction were weak (AUCR <2 and >0.5, respectively), the values after offset could be used to avoid clinical DDI studies. We did not include strong perpetrators in this study, thus the offsets of strong inhibition and induction should be evaluated in the future. Static models also showed relatively good predictability (Fig. 3B); however, there are some compounds with predicted strong inhibition and induction, and in these cases, it is difficult to judge whether clinical studies are not necessary (Fig. 5B). The balance between inhibition and induction varies with the timing of the administration of a perpetrator and a substrate. In this study, the same timing was used as in the referred clinical study, and in some studies, midazolam was administered 0.5–2 hours later than the perpetrator (Supplemental Table 1). The offset of TDI and induction was less affected by the timing of administration; however, in the offset of reversible inhibition and induction, inhibition was predicted to be weak by the delayed administration of midazolam (unpublished data). Therefore, PBPK models should be used for not only discussing the necessity of clinical studies but also the design.

In conclusion, our study demonstrates the importance of intestinal DDIs when assessing weak DDIs via CYP3A. It indicates that PBPK models are able to reasonably predict weak DDIs via intestinal CYP3A without underestimation by incorporating all of the mechanisms, including reversible inhibition, TDI, and induction. PBPK model can be used to judge the necessity of clinical DDI studies for CYP3A perpetrators, even with both inhibition and induction, and to avoid unnecessary clinical trials that burden subjects, ensuring the safety of patients.

Acknowledgments

The authors thank Daiichi Sankyo R.D. Novare for supporting the studies of in vitro physicochemical properties of perpetrator drugs and Sekisui Medical for supporting the CYP3A4 induction study. The authors also thank Dr. Michael Bolger and Dr. Viera Lukacova (Simulations Plus) and Professor Kiyomi Ito (Musashino University) for their expert advice.

Authorship Contributions

Participated in research design: Yamada, Inoue, Sugiyama, Nishiya, Ishizuka, A. Watanabe.

Conducted experiments: Yamada.

Performed data analysis: Yamada, Sugiyama, Nishiya.

Wrote or contributed to the writing of the manuscript: Yamada, Inoue, Sugiyama, Nishiya, Ishizuka, A. Watanabe, K. Watanabe, Yamashita, N. Watanabe.

References

Aasa J, Hu Y, Eklund G, Lindgren A, Baranczewski P, Malmquist J, Turek D, and Bueters T (2013) Effect of solvents on the time-dependent inhibition of CYP3A4 and the biotransformation of AZD3839 in human liver microsomes and hepatocytes. *Drug Metab Dispos* **41**:159–169.

Agoram B, Woltosz WS, and Bolger MB (2001) Predicting the impact of physiological and biochemical processes on oral drug bioavailability. *Adv Drug Deliv Rev* **50** (Suppl 1):S41–S67.

Andersin R (1991) Solubility and acid-base behaviour of midazolam in media of different pH, studied by ultraviolet spectrophotometry with multicomponent software. *J Pharm Biomed Anal* **9**:451–455.

Austin RP, Barton P, Mohmed S, and Riley RJ (2005) The binding of drugs to hepatocytes and its relationship to physicochemical properties. *Drug Metab Dispos* **33**:419–425.

Fahmi OA, Maurer TS, Kish M, Cardenas E, Boldt S, and Nettleton D (2008) A combined model for predicting CYP3A4 clinical net drug-drug interaction based on CYP3A4 inhibition, inactivation, and induction determined in vitro. *Drug Metab Dispos* **36**:1698–1708.

Food and Drug Administration (2017) Guidance for industry: in vitro metabolism- and transporter-mediated drug-drug interaction studies (draft guidance), US Department of Health and Human Services Center for Drug Evaluation and Research, FDA, Silver Spring, MD.

Galetin A, Gertz M, and Houston JB (2008) Potential role of intestinal first-pass metabolism in the prediction of drug-drug interactions. *Expert Opin Drug Metab Toxicol* **4**:909–922.

Galetin A, Hinton LK, Burt H, Obach RS, and Houston JB (2007) Maximal inhibition of intestinal first-pass metabolism as a pragmatic indicator of intestinal contribution to the drug-drug interactions for CYP3A4 cleared drugs. *Curr Drug Metab* **8**:685–693.

Gertz M, Harrison A, Houston JB, and Galetin A (2010) Prediction of human intestinal first-pass metabolism of 25 CYP3A substrates from in vitro clearance and permeability data. *Drug Metab Dispos* **38**:1147–1158.

Gertz M, Houston JB, and Galetin A (2011) Physiologically based pharmacokinetic modeling of intestinal first-pass metabolism of CYP3A substrates with high intestinal extraction. *Drug Metab Dispos* **39**:1633–1642.

Greenblatt DJ (2014) In vitro prediction of clinical drug interactions with CYP3A substrates: we are not there yet. *Clin Pharmacol Ther* **95**:133–135.

Guest EJ, Aarons L, Houston JB, Rostami-Hodjegan A, and Galetin A (2011) Critique of the two-fold measure of prediction success for ratios: application for the assessment of drug-drug interactions. *Drug Metab Dispos* **39**:170–173.

Haarhoff ZE, Kramer MA, Zvyaga TA, Zhang J, Bhutani P, Subramanian M, and Rodrigues AD (2017) Comprehensive evaluation of liver microsomal cytochrome P450 3A (CYP3A) inhibition: comparison of cynomolgus monkey and human. *Xenobiotica* **47**:470–478.

Hallifax D and Houston JB (2006) Binding of drugs to hepatic microsomes: comment and assessment of current prediction methodology with recommendation for improvement. *Drug Metab Dispos* **34**:724–726, author reply 727.

Heikkinen AT, Baneyx G, Caruso A, and Parrott N (2012) Application of PBPK modeling to predict human intestinal metabolism of CYP3A substrates - an evaluation and case study using GastroPlus. *Eur J Pharm Sci* **47**:375–386.

Hsueh C-H, Hsu V, Pan Y, and Zhao P (2018) Predictive performance of physiologically-based pharmacokinetic models in predicting drug-drug interactions involving enzyme modulation. *Clin Pharmacokinet* **57**:1337–1346.

Mao J, Tay S, Khojasteh CS, Chen Y, Hop CE, and Kenny JR (2016) Evaluation of time dependent inhibition assays for marketed oncology drugs: comparison of human hepatocytes and liver microsomes in the presence and absence of human plasma. *Pharm Res* **33**:1204–1219.

Nishiya Y, Nakamura K, Okudaira N, Abe K, Kobayashi N, and Okazaki O (2010) Effects of organic solvents on the time-dependent inhibition of CYP3A4 by diazepam. *Xenobiotica* **40**:1–8.

Prueksaritanont T, Chu X, Gibson C, Cui D, Yee KL, Ballard J, Cabalu T, and Hochman J (2013) Drug-drug interaction studies: regulatory guidance and an industry perspective. *AAPS J* **15**: 629–645.

Rostami-Hodjegan A and Tucker G (2004) 'In silico' simulations to assess the 'in vivo' consequences of 'in vitro' metabolic drug-drug interactions. *Drug Discov Today Technol* **1**:441–448.

Thummel KE, O'Shea D, Paine MF, Shen DD, Kunze KL, Perkins JD, and Wilkinson GR (1996) Oral first-pass elimination of midazolam involves both gastrointestinal and hepatic CYP3A-mediated metabolism. *Clin Pharmacol Ther* **59**:491–502.

Vieira ML, Kirby B, Ragueneau-Majlessi I, Galetin A, Chien JY, Einolf HJ, Fahmi OA, Fischer V, Fretland A, Grime K, et al. (2014) Evaluation of various static in vitro-in vivo extrapolation models for risk assessment of the CYP3A inhibition potential of an investigational drug. *Clin Pharmacol Ther* **95**:189–198.

Yang J, Jamei M, Yeo KR, Tucker GT, and Rostami-Hodjegan A (2007) Prediction of intestinal first-pass drug metabolism. *Curr Drug Metab* **8**:676–684.

Zhang X, Quinney SK, Gorski JC, Jones DR, and Hall SD (2009) Semiphysiologically based pharmacokinetic models for the inhibition of midazolam clearance by diltiazem and its major metabolite. *Drug Metab Dispos* **37**:1587–1597.

Zhou ZW and Zhou SF (2009) Application of mechanism-based CYP inhibition for predicting drug-drug interactions. *Expert Opin Drug Metab Toxicol* **5**:579–605.

Zimmerlin A, Trunzer M, and Faller B (2011) CYP3A time-dependent inhibition risk assessment validated with 400 reference drugs. *Drug Metab Dispos* **39**:1039–1046.

Address correspondence to: Makiko Yamada, Drug Metabolism and Pharmacokinetics Research Laboratories, Daiichi Sankyo Co., Ltd., 1-2-58, Hiromachi, Shinagawa-ku, Tokyo 140-8710, Japan. E-mail: yamada.makiko.jr@daiichisankyo.co.jp

Drug Metabolism and Disposition

Supplemental Data

Critical impact of drug-drug interactions via intestinal CYP3A in the risk assessment of weak perpetrators using physiologically based pharmacokinetic models

Makiko Yamada, Shin-ichi Inoue, Daisuke Sugiyama, Yumi Nishiya, Tomoko Ishizuka, Akiko Watanabe, Kengo Watanabe, Shinji Yamashita, Nobuaki Watanabe

Drug Metabolism and Pharmacokinetics Research Laboratories, Daiichi Sankyo Co., Ltd., Tokyo, Japan (M.Y., S.I., D.S., Y.N., T.I., A.W., K.W., N.W.) and Faculty of Pharmaceutical Sciences, Setsunan University, Osaka, Japan (S.Y.)

Supplemental Methods

Search for product labels of DDI studies with midazolam in PharmaPendium

A product label information search was conducted on March 5, 2019, using PharmaPendium (Elsevier, Amsterdam, Netherlands), a database of drug approval documents. Using the metabolizing enzyme and transported module, the compounds were extracted with following settings:

Data types: Enzyme inhibitor (in vivo) and enzyme inducer (in vivo)
Enzyme/transporter name: CYP3A
Species: Human
Sources: Label in FDA approval packages

The search results were exported to Microsoft Excel 2013 (Microsoft Corporation, Redmond, WA), and the midazolam DDI studies were extracted and manually checked. Among the extracted labels, the oldest was published in 2003. When a change in the AUC of midazolam was described in the label, the drugs with AUCR of 0.8–1.25 were categorized as DDI negative, and others were positive. For the drugs with no specific values included, the expression of positive or negative DDIs written on the label was used for the categorization. When both the positive and negative results were included for one compound, it was categorized as a positive result. As a result, 83 drugs were found to include a midazolam DDI study in their label, and 36 and 47 drugs were categorized as positive and negative drugs, respectively.

In vitro DDI study

CYP3A inhibition

The composition of reaction mixture for inhibition constant (K_i) calculation was as follows: human liver microsomes (final concentration: 0.02 mg protein/mL), potassium phosphate buffer (pH 7.4, 0.1 M), midazolam (2, 4, and 8 μM), NADPHgs (5% for NADPH Regeneration System Solution A and 1% for NADPH Regeneration System Solution B), and marketed drugs. The concentrations of the test substances are as follows: 0.25, 0.5, and 1 μM for everolimus, felodipine, and simvastatin; 2, 5, and 10 μM for casopitant, fluoxetine, fluvoxamine, pazopanib, and suvorexant; 10, 20, and 50 μM for ethinyl estradiol; 20, 50, and 100 μM for atomoxetine, atorvastatin, roxithromycin, and tadalafil; and 200, 500, and 1000 μM for azithromycin, cimetidine, deferasirox, and ranitidine. For inactivation parameter determination, the composition of the reaction mixture was similar to above, except the concentrations of human liver microsomes (0.2 mg protein/mL), midazolam (40 μM), and test substances (1 to 100 μM) were different. When the test substances were dissolved, to increase solubility, small

amounts of HCl and NaOH were added to the pazopanib and deferasirox solutions, respectively.

Liquid chromatography was performed using an Acquity Ultra Performance LC (Waters, Milford, MA) system: chromatographic separation was conducted on an ACQUITY UPLC HSS T3 column (1.7 μm, 2.1 mm I.D. × 50 mm, Waters) in an oven set at 50 °C. The autosampler temperature was maintained at 5 °C. The mobile phase consisted of two solvents: A (acetonitrile containing 5 mM ammonium acetate and 0.2% formic acid) and B (water containing 5 mM ammonium acetate and 0.2% formic acid). Separations were achieved using a gradient elution. Mass spectrometric detection was performed using a TQ Detector (Waters) with an electrospray ionization (ESI) interface. The source temperature was maintained at 150 °C and the desolvation temperature was maintained at 450 °C. Quantification was performed using the peak area ratio. Data acquisition and processing were conducted using MassLynx 4.1 SCN 714 (Waters).

CYP3A4 induction

The final concentration range of the test substances were as follows: 0.001 to 1 μM for everolimus, 0.03 to 30 μM for atomoxetine, azithromycin, casopitant, felodipine, and roxithromycin; and 0.1 to 100 μM for cimetidine, deferasirox, fluvoxamine, pazopanib, ranitidine, simvastatin, and tadalafil. Rifampicin (10 μM) and omeprazole (50 μM) were used as positive controls, and gatifloxacin (10 μM) was used as the negative control. The hepatocytes were prepared using the OptiTHAW hepatocyte isolation kit (Sekisui XenoTech) at 6×10^5 hepatocytes/mL in modified Lanford medium containing 10% fetal bovine serum. A 100 μL sample of the cell suspension was seeded into each well of a 96-well culture plate (BioCoat Collagen, Corning) and cultured for 4–6 h in a CO_2 incubator (37 °C, 5% CO_2). Subsequently, the medium was replaced with 100 μL of modified Lanford medium, and the cells were cultured overnight. On the next day, the incubation medium was replaced with the medium containing the test or control substances, and the plate was cultured overnight. This operation was repeated, which resulted in a total treatment time of 48 h. All determinations were performed in triplicate. After the incubation with the test and control substances, the hepatocyte cultures were washed with phosphate-buffered saline and total RNA was extracted using the RNeasy 96 Kit (Qiagen, Hilden, Germany). To prepare the calibration curve, Human Liver Total RNA (Clontech Laboratories, Mountain View, CA) was diluted with water to 20 μg/mL in the absence of RNase, and then further diluted with 50 μg/mL yeast tRNA (Thermo Fisher Scientific, Waltham, MA) to concentrations between 0.256 and 20000 ng/mL. For the reverse transcription-polymerase chain reaction (RT-PCR), TaqMan Fast Virus 1-Step Master Mix (Thermo Fisher Scientific) containing 500 nM forward primer, 500 nM reverse primer, and 200 nM TaqMan probe was used. The forward and reverse primers and TaqMan probes were purchased from Sigma-Aldrich, with the following sequences, respectively: for CYP3A4, 5'-GATTGACTCTCAGAATTCAAAAGAAACTGA-3' and 5'-

GGTGAGTGGCCAGTTCATACATAATG-3', and 5'-AGGAGAGAACACTGCTCGTGGTTTCACAG-3'; and for glyceraldehyde-3-phosphate dehydrogenase (GAPDH), 5'-CCACCCATGGCAAATTCC-3', 5'-GATGGGATTTCCATTGATGACA-3', and 5'-TGGCACCGTCAAGGCTGAGAACG-3'. The amplification and detection were performed using the PRISM 7900HT (Thermo Fisher Scientific) or QuantStudio7 (Thermo Fisher Scientific) with the following profile: 1 cycle at 50 °C for 30 s; 1 cycle at 95 °C for 20 s; and 40 cycles each at 95 °C for 1 s; and 60 °C for 20 s. The mRNA expression for each gene was calculated as the amount of human liver total RNA used for the calibration curve.

QuantStudio 7 operating and data analysis software was used to create a calibration curve and calculate the mRNA expression. The mRNA expression was calculated by the division of the mRNA expression of CYP3A4 by the mRNA expression of GAPDH.

Supplemental Table 1 Clinical DDI studies used in the prediction

Precipitant	Observed AUCR	Precipitant dose	Midazolam dose	Midazolam dosing time	Reference
atomoxetine	1.20	60 mg (12 days), b.i.d.	5 mg	0.5 h	Sauer *et al.*, 2004
atorvastatin	1.15	10 mg (14 days), q.d.	0.15 μg/kg	0 h	Kokudai *et al.*, 2009
azithromycin	1.19	500 mg (3 days), q.d.	15 mg	1.5 h	Yeates *et al.*, 1996
casopitant	1.46	10 mg (3 days), q.d.	5 mg	1 h	Zamuner *et al.*, 2010
cimetidine	1.35	400 mg (2 days), b.i.d.	15 mg	0.5 h	Fee *et al.*, 1987
deferasirox	0.90	30 mg/kg (4 days), q.d.	5 mg	1 h	Skerjanec *et al.*, 2010
ethinyl estradiol	1.10	0.03 mg (10 days), q.d.	3 mg	0 h	Belle *et al.*, 2002
everolimus	1.31	10 mg (5 days), q.d.	4 mg	0 h	Urva *et al.*, 2013
felodipine	1.23	10 mg (7 days), q.d.	2 mg	1 h	Snyder *et al.*, 2014
fluoxetine	0.84	20 mg (12 days), q.d.	10 mg	1 h	Lam *et al.*, 2003
fluvoxamine	1.39	100 mg (12 days), b.i.d.	10 mg	1 h	Lam *et al.*, 2003
pazopanib	1.32	800 mg (17 days), q.d.	3 mg	0 h	Goh *et al.*, 2010
ranitidine	1.23	150 mg (2 days), b.i.d	15 mg	0.5 h	Fee *et al.*, 1987
roxithromycin	1.47	300 mg (6 days), q.d.	15 mg	2 h	Backman *et al.*, 1994
simvastatin	1.24	10 mg (14 days), q.d.	0.15 μg/kg	0 h	Kokudai *et al.*, 2009
suvorexant	1.47	80 mg (14 days), q.d.	2 mg	2 h	NDA 204569
tadalafil	0.90	10 mg (14 days), q.d.	15 mg	0 h	Ring *et al.*, 2005

When the dosing time of midazolam was unclear from the literature, simultaneous administration with a perpetrator was assumed. When the dose per body weight was given, 70 kg body weight was assumed.

Supplemental Table 2 Inhibition constants (K_i), inactivation rate constant (k_{inact}), and the concentration at half k_{inact} (K_I) for CYP3A in human liver microsomes from the literature**.**

Precipitant	Reversible inhibition		Time-dependent inhibition		
	K_i (μM)	Reference	K_I (μM)	k_{inact} (/min)	Reference
atomoxetine	34	Sauer *et al.*, 2004	-	-	
atorvastatin	12.4	Mc Donnell *et al.*, 2005	-	-	
azithromycin	85[a]	Gascon and Dayer, 1991	105	0.0102	Rowland Yeo *et al.*, 2011
casopitant	4.93[a]	Motta *et al.*, 2011	3.1	0.0199	Motta *et al.*, 2011
cimetidine	275[a]	Gascon and Dayer, 1991	-	-	
deferasirox	100[a]	Skerjanec *et al.*, 2010	-	-	
ethinyl estradiol	21[a]	Chang *et al.*, 2009	58.6	0.254	Zimmerlin *et al.*, 2011
everolimus	-		0.9	0.022	Kenny *et al.*, 2012
felodipine	0.25	Foti *et al.*, 2010	-	-	
fluoxetine	11.5	von Moltke *et al.*, 1996	8.6	0.005	Albaugh *et al.*, 2012
fluvoxamine	21.5[a]	Obach *et al.*, 2006	-	-	
pazopanib	6[a]	pazopanib NDA 022465	2.9	0.021	Mao *et al.*, 2016
ranitidine	-		-	-	
roxithromycin	34[a]	Obach *et al.*, 2006	72	0.023	Fahmi *et al.*, 2008
simvastatin	0.385[a]	Obach *et al.*, 2006	4.6	0.006	Zimmerlin *et al.*, 2011
suvorexant	2[a]	Cui *et al.*, 2016	11.6	0.136	suvorexant NDA 204569
tadalafil	41	Ring *et al.*, 2005	27.5	0.228	Zimmerlin *et al.*, 2011

-, no value was found in the Drug Interaction Database (https://www.druginteractioninfo.org, University of Washington, Seattle, WA)

a, the value is one half of IC_{50}

Supplemental Table 3 k_a, R_b, F_a, AUC, and C_{max} used for the mechanistic static analysis

	k_a (1/h)	R_b	F_a	AUC_{inf} (ng·h/mL)	C_{max} (ng/mL)	Reference
atomoxetine	2.29	0.93	1.00	15400	1710	Todor *et al.*, 2016
atorvastatin	1.67	0.49	1.00	25.6	3.53	Yamazaki *et al.*, 2017
azithromycin	0.435	0.66	0.54	2550	289	Cook *et al.*, 2006
casopitant	0.503	0.69	1.00	391	66.0	Pellegatti *et al.*, 2009
cimetidine	0.371	0.78	0.84	11600	1860	Tiseo *et al.*, 1998
deferasirox	0.736	0.78	1.00	543000	42440	Skerjanec *et al.*, 2010
ethinyl estradiol	1.88	0.95	1.00	0.683	0.0679	Marshall *et al.*, 2017
everolimus	5.96	0.62	1.00	324	31.0	Peveling-Oberhag *et al.*, 2013
felodipine	0.817	0.62	0.93	25.3	2.20	Edgar *et al.*, 1987
fluoxetine	0.442	0.87	1.00	850	44.0	Zhi *et al.*, 2003
fluvoxamine	0.512	0.86	1.00	1171	107	Fleishaker and Hulst, 1994
pazopanib	1.17	0.88	0.13	1260000	48900	Heath *et al.*, 2012
ranitidine	0.411	0.78	0.92	2540	474	van Crugten *et al.*, 1986
roxithromycin	1.23	0.64	0.59	151000	14230	Hang *et al.*, 2007
simvastatin	1.83	0.75	1.00	4.32	0.635	Wu *et al.*, 2016
suvorexant	2.17	0.69	1.00	9750	1180	Cui *et al.*, 2016
tadalafil	1.31	0.70	0.98	2450	189	Ring *et al.*, 2005

k_a was calculated using the concentration-time profile of each drug from literature (reference) by Phoenix WinNonlin. R_b was predicted by ADMET predictor. F_a and AUC_{inf} after single dose and C_{max} after multiple doses were calculated by GastroPlus with the doses summarized in Supplemental Table 1.

Supplemental Table 4 Fraction unbound, adjusted fraction unbound in plasma, and fraction unbound during incubation

Precipitant	$f_{u,p}$	Data Source of $f_{u,p}$	$f_{u,p,adj}$	$f_{u,inc}$		
				Reversible inhibition	Time-dependent inhibition	Induction
atomoxetine	0.02	DIDB	0.020	0.967	-	-
atorvastatin	0.02	DIDB	0.018	0.989	0.898	0.588
azithromycin	0.94	In-house	0.92	-	0.944	-
casopitant	0.0060	In-house	0.0029	0.921	0.538	0.275
cimetidine	0.81	DIDB	0.80	0.998	0.984	-
deferasirox	0.01	DIDB	0.010	0.998	0.985	-
ethinyl estradiol	0.054	ADMET predictor	0.021	0.976	0.803	0.450
everolimus	0.078	ADMET predictor	0.00045	0.628	0.144	0.125
felodipine	0.004	DIDB	0.0035	0.971	0.772	0.420
fluoxetine	0.06	DIDB	0.059	0.959	0.702	0.365
fluvoxamine	0.23	DIDB	0.22	0.987	0.882	0.557
pazopanib	0.002	In-house	0.0019	0.978	0.817	0.466
ranitidine	0.85	DIDB	0.85	0.998	0.984	-
roxithromycin	0.05	(Chantot *et al.*, 1986)	0.05	0.989	0.901	-
simvastatin	0.06	DIDB	0.0032	0.896	0.462	0.244
suvorexant	0.005	In-house	0.0034	0.949	0.652	0.334
tadalafil	0.06	DIDB	0.059	0.997	0.970	0.834

$f_{u,p,adj}$, adjusted fraction unbound in plasma for possible binding to plasma lipids by GastroPlus; $f_{u,inc}$, fraction unbound during incubation predicted by GastroPlus; DIDB, Drug Interaction Database

Supplemental Table 5 Solubility, pKa, and bile salt solubilization ratio (BSSR) of perpetrators used for the simulation

	Reference solubility (mg/mL)	pH[a]	Data source	pKa1[b]	pKa2[b]	BSSR[c]
atomoxetine	27.8	11.4	PubChem (water)	9.72 (base)	-	0
atorvastatin	1.23	6.0	PubChem	11.05 (acid)	4.71 (acid)	0
azithromycin	0.514	9.76	PubChem (water)	8.72 (base)	7.63 (base)	0
casopitant	0.034	6.8	In-house	6.74 (base)	-	0
cimetidine	9.38	8.79	PubChem (water)	6.85 (base)	4.16 (base)	0
deferasirox	0.33	6.8	In-house	8.75 (acid)	3.8 (acid)	1.4E+05
ethinyl estradiol	0.0113	6.98	PubChem (water)	10.32 (acid)	-	3.9E+04
everolimus	0.008	7	ADMET predictor	-	-	2.2E+05
felodipine	0.0034	6.8	In-house	0.51 (base)	10.95 (acid)	1.7E+05
fluoxetine	50	11.5	PubChem (water)	9.82 (base)	-	0
fluvoxamine	14.869	10.9	Kwon and Armbrust, 2008 (water)	9.05 (base)	-2.06 (base)	0
pazopanib	0.0001	6.8	In-house	5.14 (base)	3.09 (base)	1.4E+06
ranitidine	24.7	9.31	PubChem (water)	7.85 (base)	3.75 (base)	0
roxithromycin	0.283	9.45	Biradar *et al.*, 2006 (water)	8.4 (base)	1.04 (base)	0
simvastatin	0.0014	5	Serajuddin *et al.*, 1991	-	-	2.7E+05
suvorexant	0.022	6.8	In-house	2.22 (base)	0.048 (base)	2.3E+04
tadalafil	0.0032	7.00	PubChem (water)	11.47 (acid)	-	1.7E+05

a, When only water solubility was available, the pH for the solubility was calculated by the ADMET predictor; b, pKa was predicted by the ADMET predictor and when more than three pKa was predicted, only the biorelevant values are shown in this table; c, BSSR was calculated by GastroPlus

Supplemental Table 6 Permeability and lipophilicity of perpetrators used for the simulation

	P_{eff}	Data source	LogP or logD[a]	pH	Data source
atomoxetine	4.19	ADMET predictor	3.9	-	PubChem
atorvastatin	1.73	ADMET predictor	5.7	-	PubChem
azithromycin	0.27	ADMET predictor	0.7	7.4	In-house
casopitant	6.51	In-house	4.5	7.4	In-house
cimetidine	0.79	ADMET predictor	0.4	-	PubChem
deferasirox	8.18	ADMET predictor	3.52	-	PubChem
ethinyl estradiol	6.98	ADMET predictor	3.67	-	PubChem
everolimus	0.28	ADMET predictor	5.56		ADMET predictor
felodipine	3.97	ADMET predictor	3.8	-	PubChem
fluoxetine	2.71	ADMET predictor	4.05	-	PubChem
fluvoxamine	2.19	ADMET predictor	3.2	-	PubChem
pazopanib	3.62	In-house	3.6	7.4	In-house
ranitidine	1.24	ADMET predictor	0.27	-	PubChem
roxithromycin	0.27	ADMET predictor	1.7	-	PubChem
simvastatin	3.83	ADMET predictor	4.68	-	PubChem
suvorexant	6.34	ADMET predictor	4.2	7.4	In-house
tadalafil	2.98	ADMET predictor	1.7	-	PubChem

a, The values with a description for pH are logD and others are logP.

Supplemental Table 7 Summary of pharmacokinetic parameters of perpetrators used for the simulation

	CL (L/h/kg)	V_c (L/kg)	K_{12} (1/h)	K_{21} (1/h)	V_2 (L/kg)	FPE_{gut} (%)	FPE_{liver} (%)
atomoxetine	0.0558	0.363	3.73	2.93	0.463	-	-
atorvastatin	0.779	0.168	21.7	0.413	8.82	76	42
azithromycin	1.54	3.46	0.520	0.352	5.12	-	-
casopitant	0.365	1.28	0.470	0.138	4.34	-	-
cimetidine	0.420	1.40	-	-	-	-	-
deferasirox	0.0553	0.683	0.099	0.920	0.0737	-	-
ethinyl estradiol	0.265	1.62	0.282	0.231	1.97	46	32
everolimus	0.0746	0.0310	5.91	0.0847	2.17	78	23
felodipine	0.79	1.47	1.28	0.849	2.21	56	66
fluoxetine	0.0817	11.4	0.0377	0.00407	105	-	-
fluvoxamine	0.57	7.9	0.0099	0.00046	170	-	47
pazopanib	0.00118	0.0802	0.0279	0.0199	0.113	-	-
ranitidine	0.781	2.47	-	-	-	-	-
roxithromycin	0.0169	0.0186	2.80	0.600	0.0865	-	-
simvastatin	1.68	3.11	-	-	-	86	64
suvorexant	0.1172	0.490	0.827	0.463	0.873	-	-
tadalafil	0.0571	0.450	0.260	0.209	0.558	-	-

FPE, first pass effect; -, not calculated

Parameters in the compartmental PK model in GastroPlus were determined to fit concentration-time profile after oral administration and may be different from the actual value. FPE was calculated for the compounds that large first-pass effects are known.

Supplemental Figure 1 Reversible inhibition for CYP3A in human liver microsomes. The x-axis represents concentrations of midazolam and the y-axis represents the midazolam 1'-hydroxylation activity. The numbers in parentheses denote the standard error.

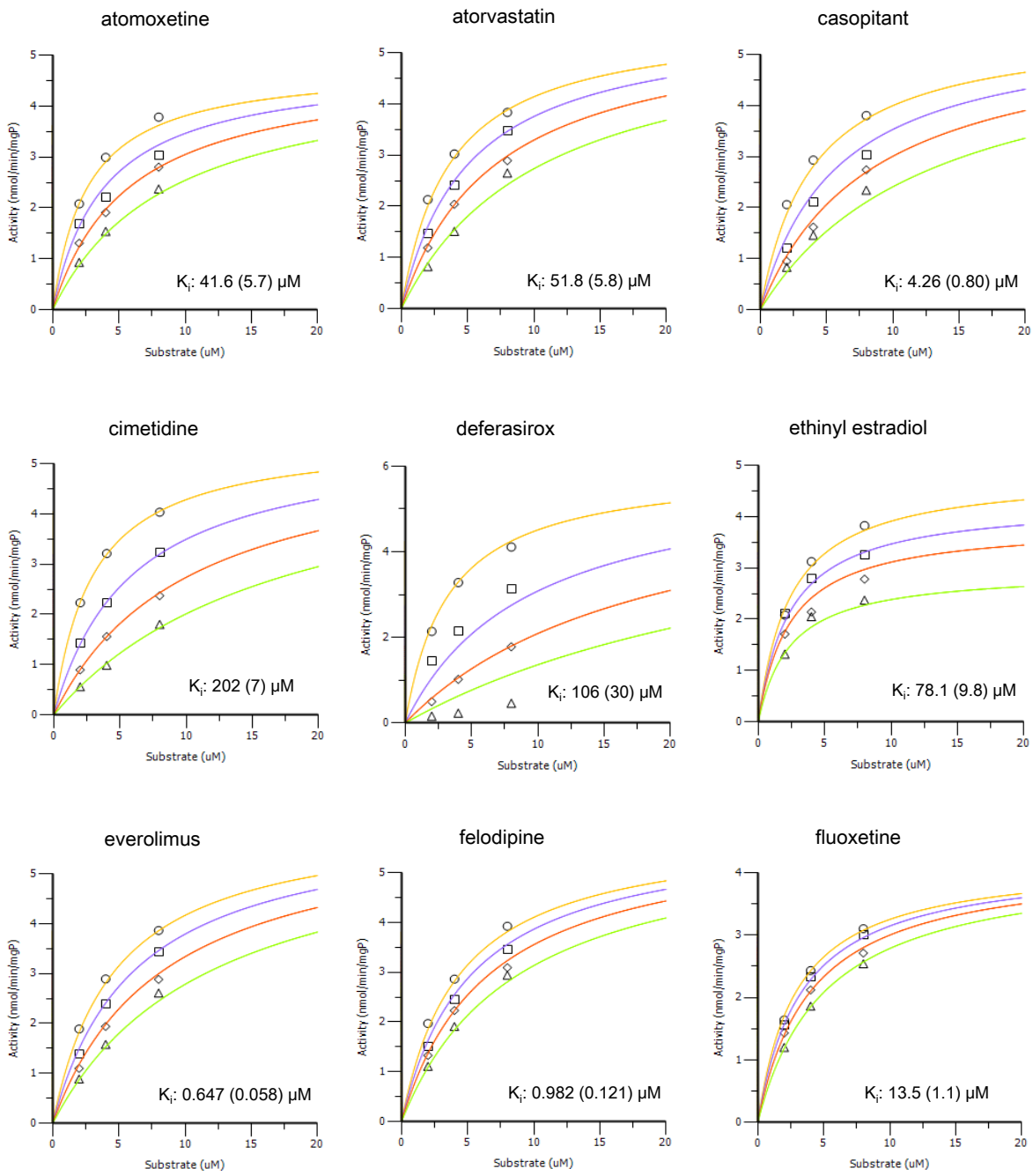

fluvoxamine

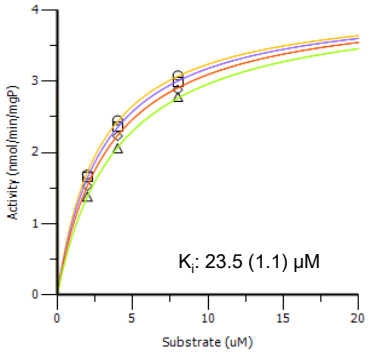

pazopanib

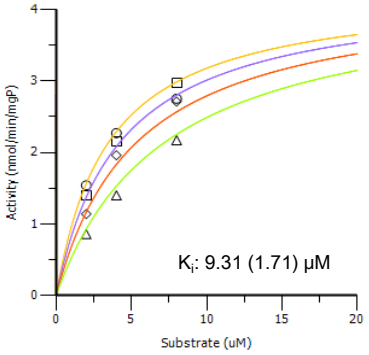

ranitidine

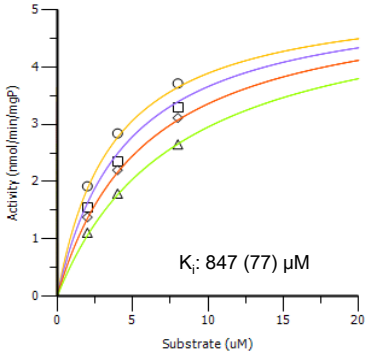

roxithromycin

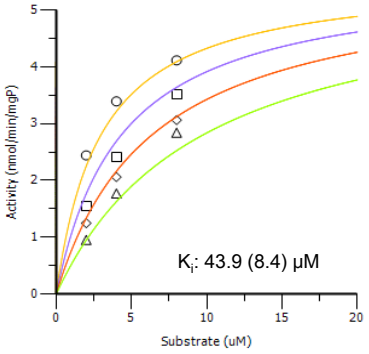

simvastatin

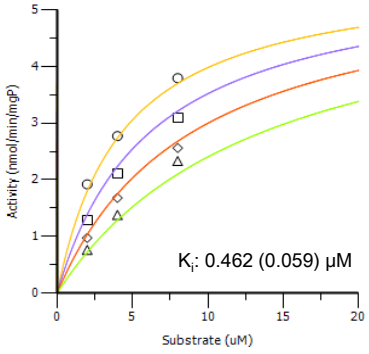

suvorexant

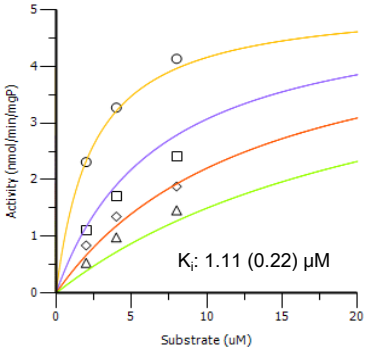

tadalafil

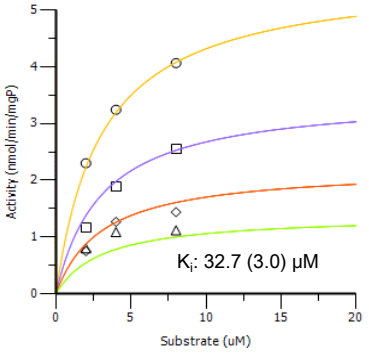

Supplemental Figure 2 Time-dependent inhibition for CYP3A in human liver microsomes. The x-axis represents concentrations of perpetrators and the y-axis represents the observed apparent inactivation rate constant, kobs. The numbers in parentheses denote the standard error.

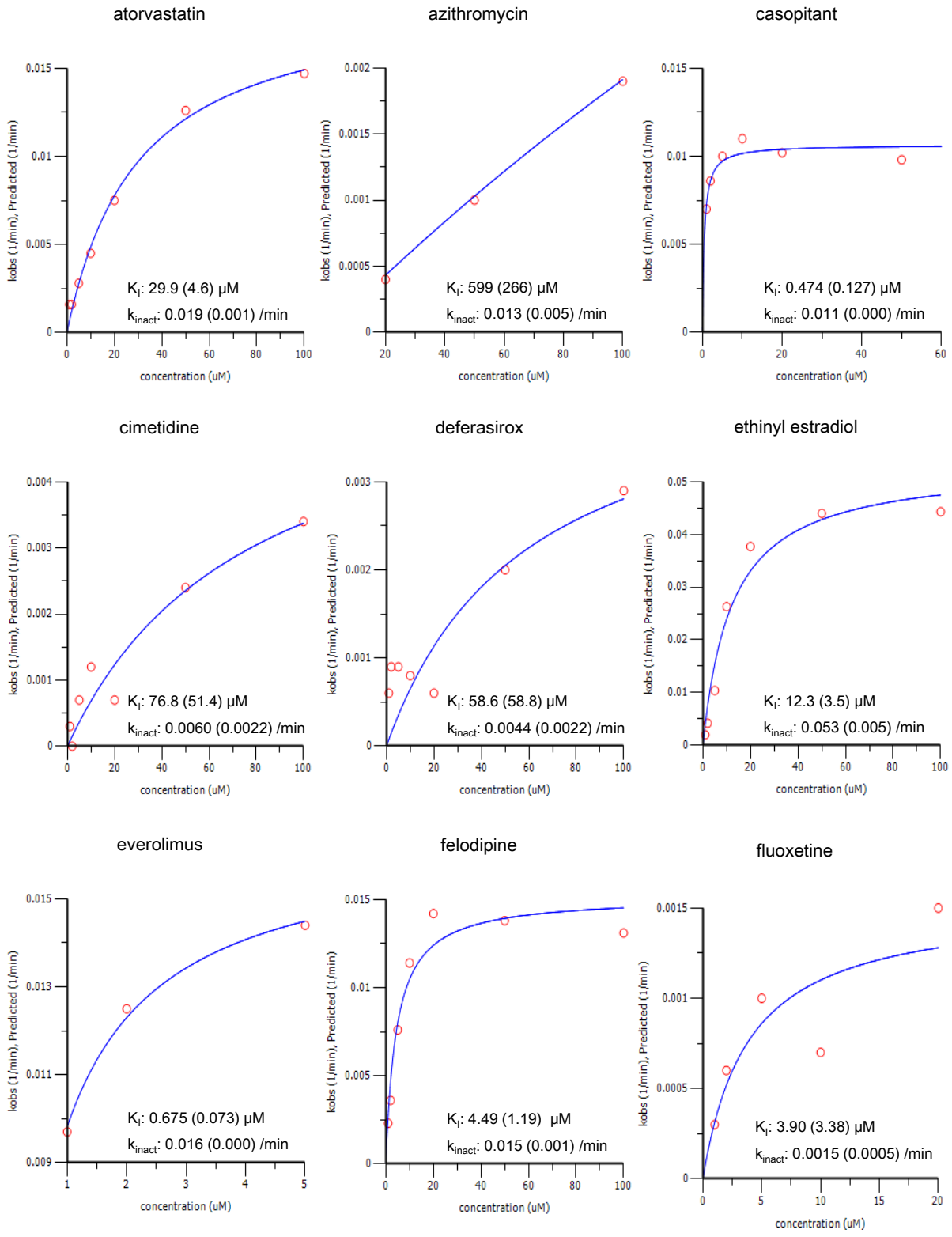

fluvoxamine

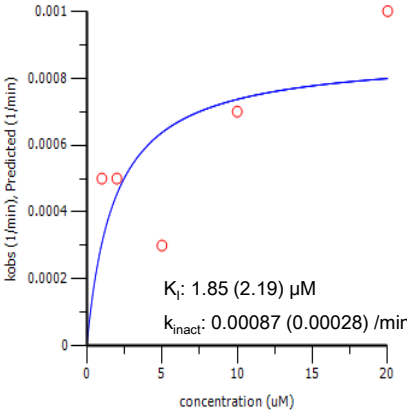

pazopanib

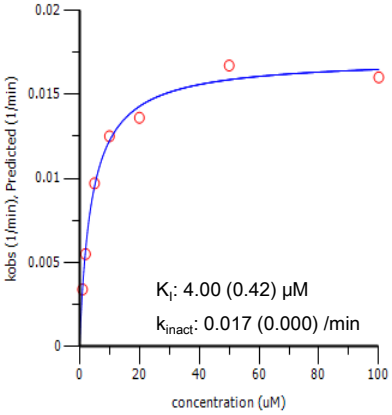

ranitidine

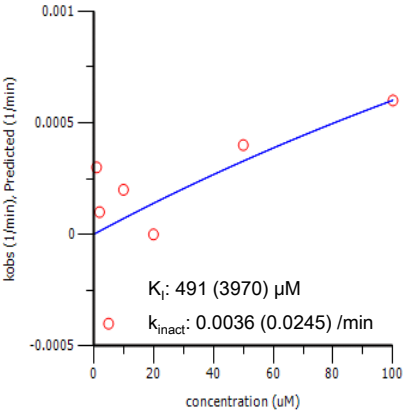

roxithromycin

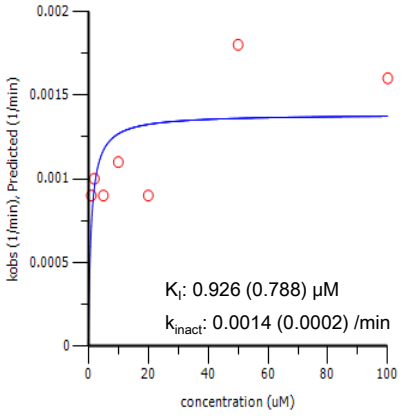

simvastatin

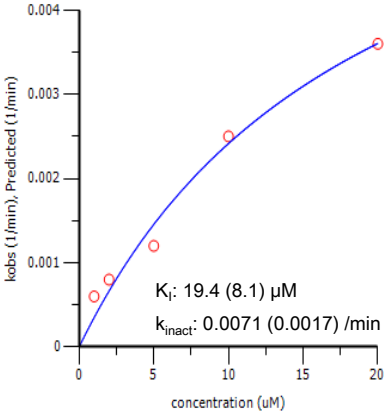

suvorexant

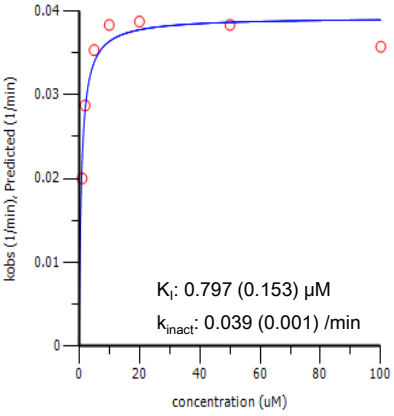

tadalafil

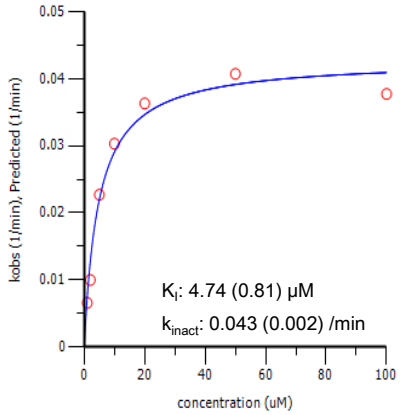

Supplemental Figure 3 Induction for CYP3A4 in human hepatocytes. The x-axis represents concentrations of perpetrators and the y-axis represents the mRNA of CYP3A4. The numbers in parentheses denote the standard error.

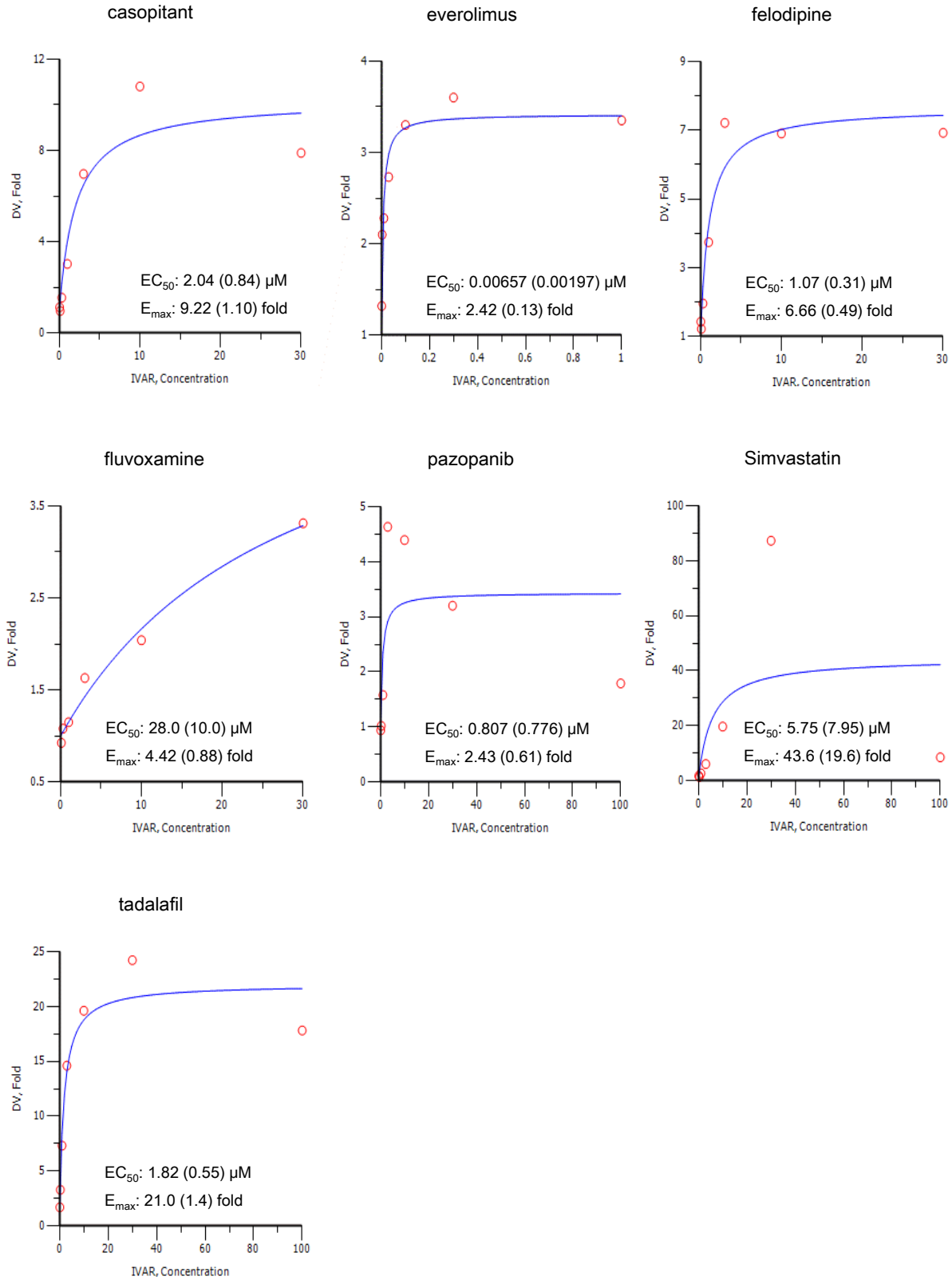

Supplemental Figure 4 Plasma concentration simulated by GastroPlus in model development. Open squares represent observed concentration in the clinical studies.

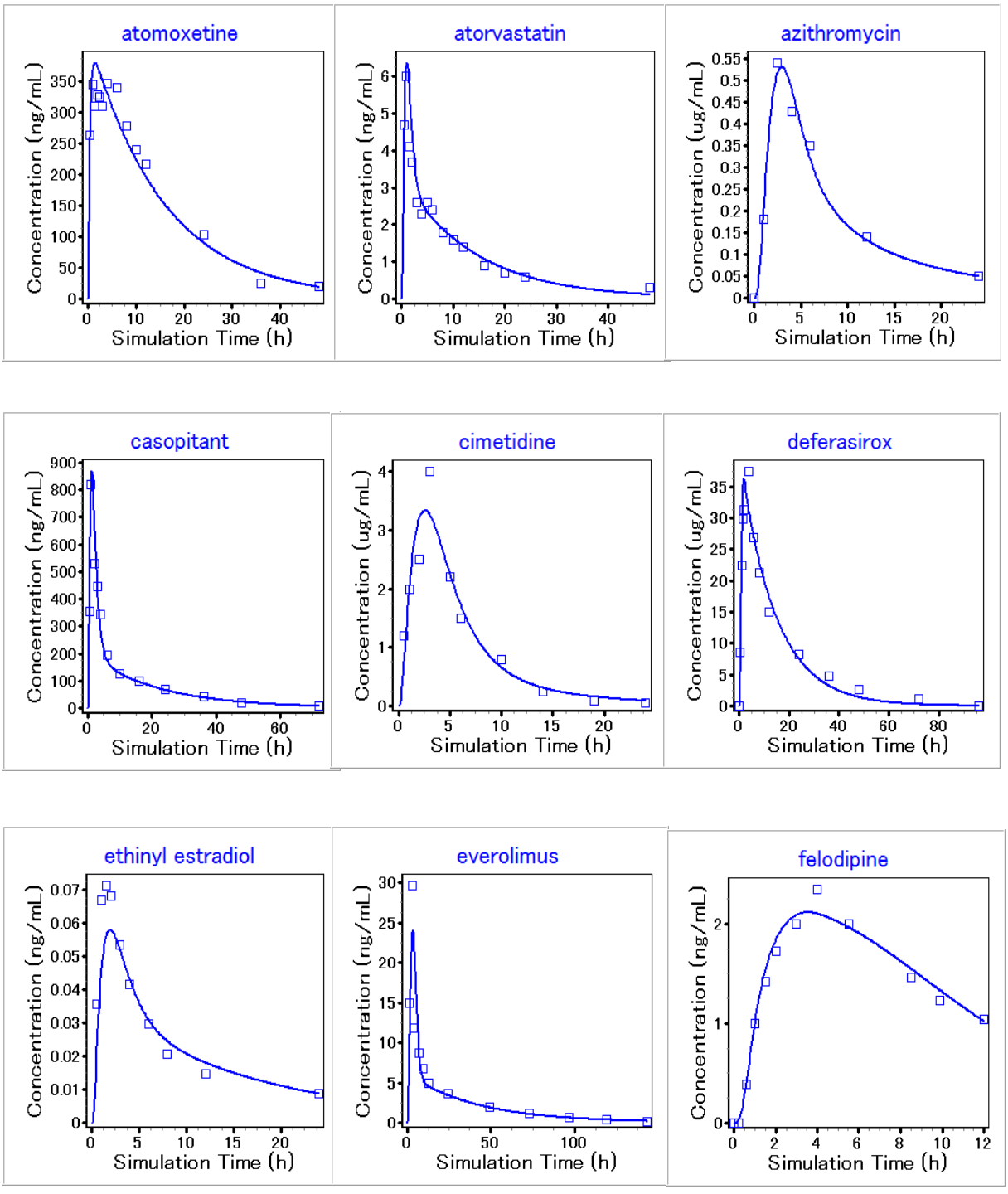

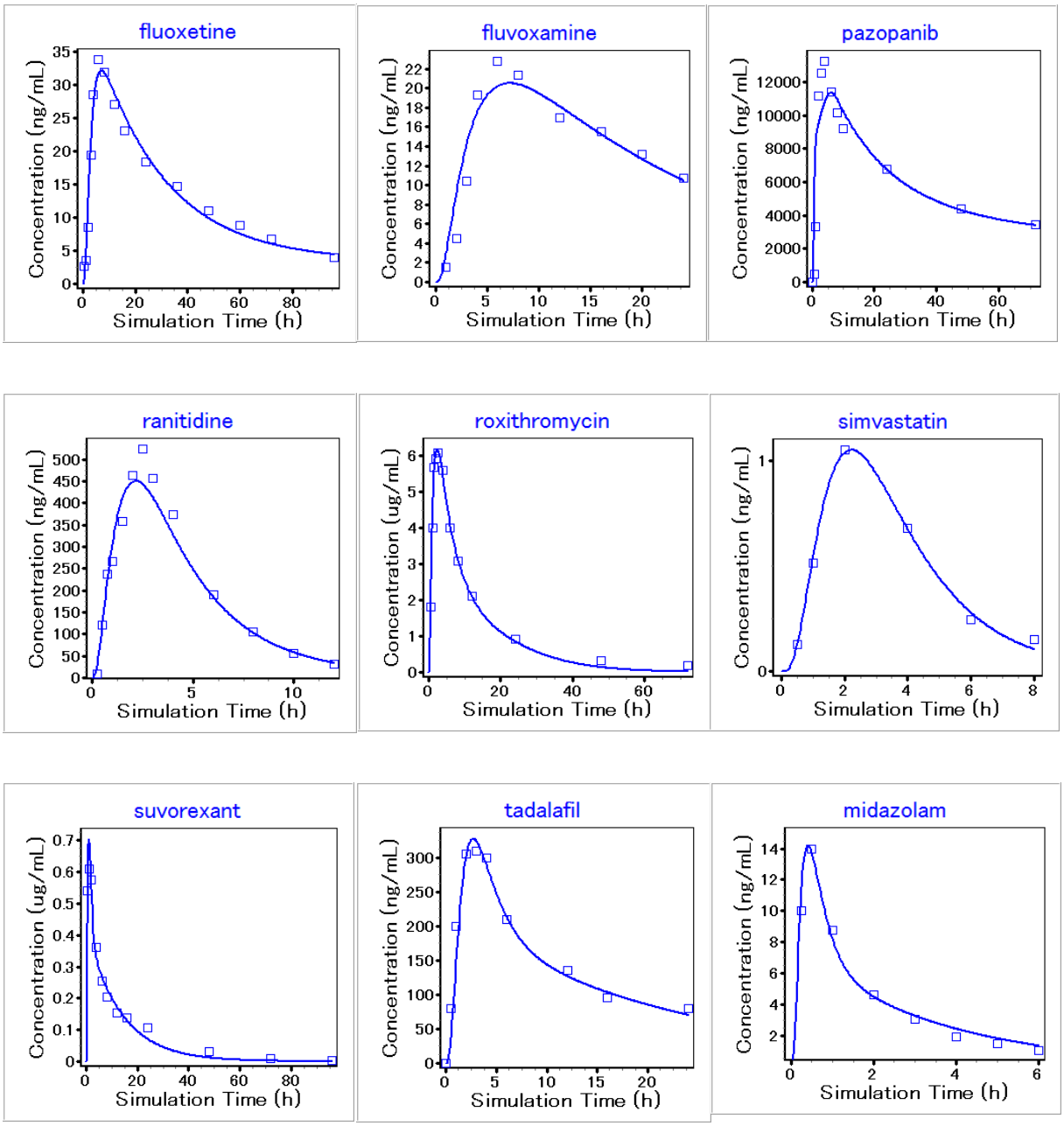
fluoxetine
Concentration (ng/mL)
Simulation Time (h)
fluvoxamine
Concentration (ng/mL)
Simulation Time (h)
pazopanib
Concentration (ng/mL)
Simulation Time (h)
ranitidine
Concentration (ng/mL)
Simulation Time (h)
roxithromycin
Concentration (ug/mL)
Simulation Time (h)
simvastatin
Concentration (ng/mL)
Simulation Time (h)
suvorexant
Concentration (ug/mL)
Simulation Time (h)
tadalafil
Concentration (ng/mL)
Simulation Time (h)
midazolam
Concentration (ng/mL)
Simulation Time (h)

Supplemental Figure 5 Concentrations in the intestine simulated by GastroPlus ($C_{ent,\ jejunum\ 1}$) and calculated for static model ($[I]_g$).

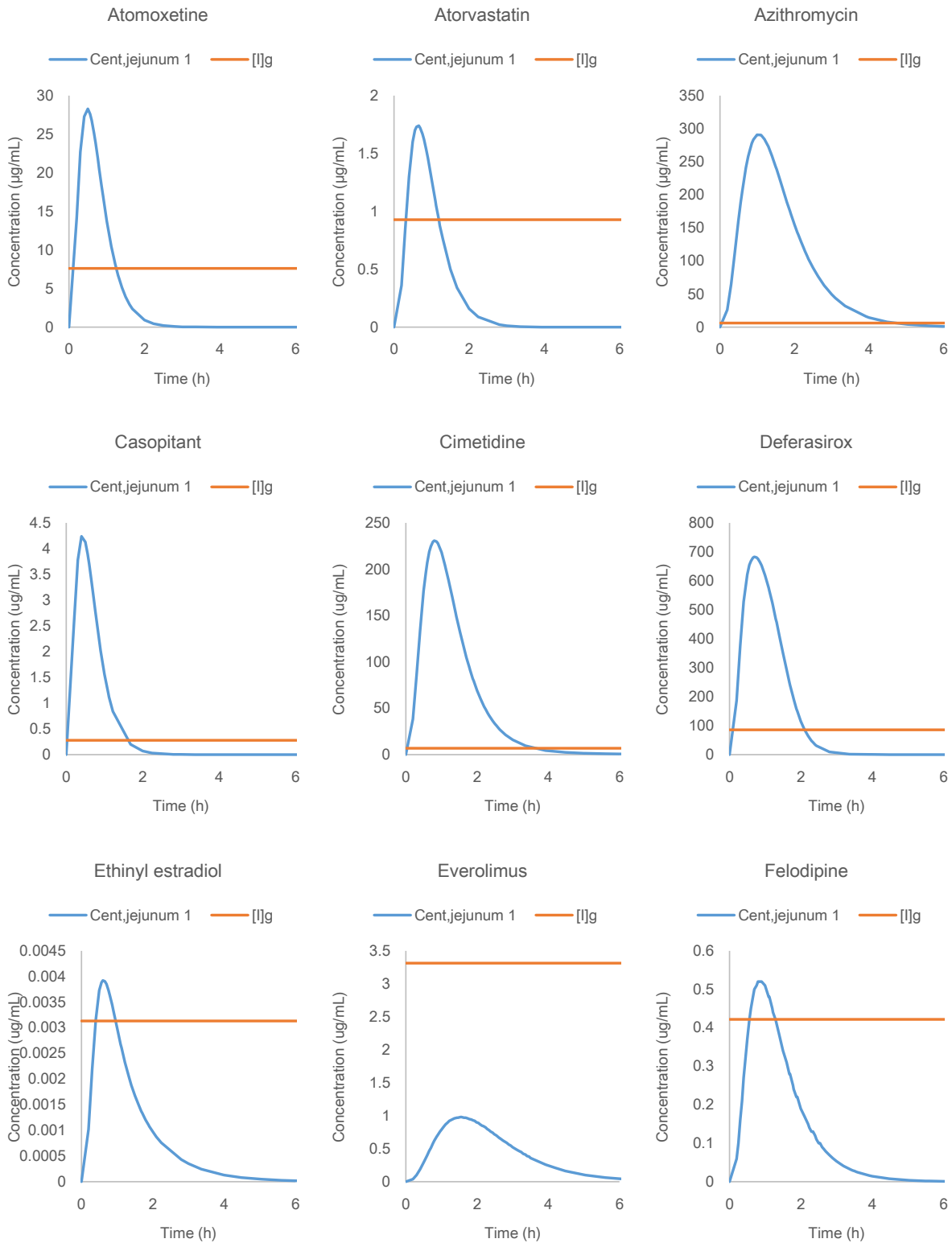

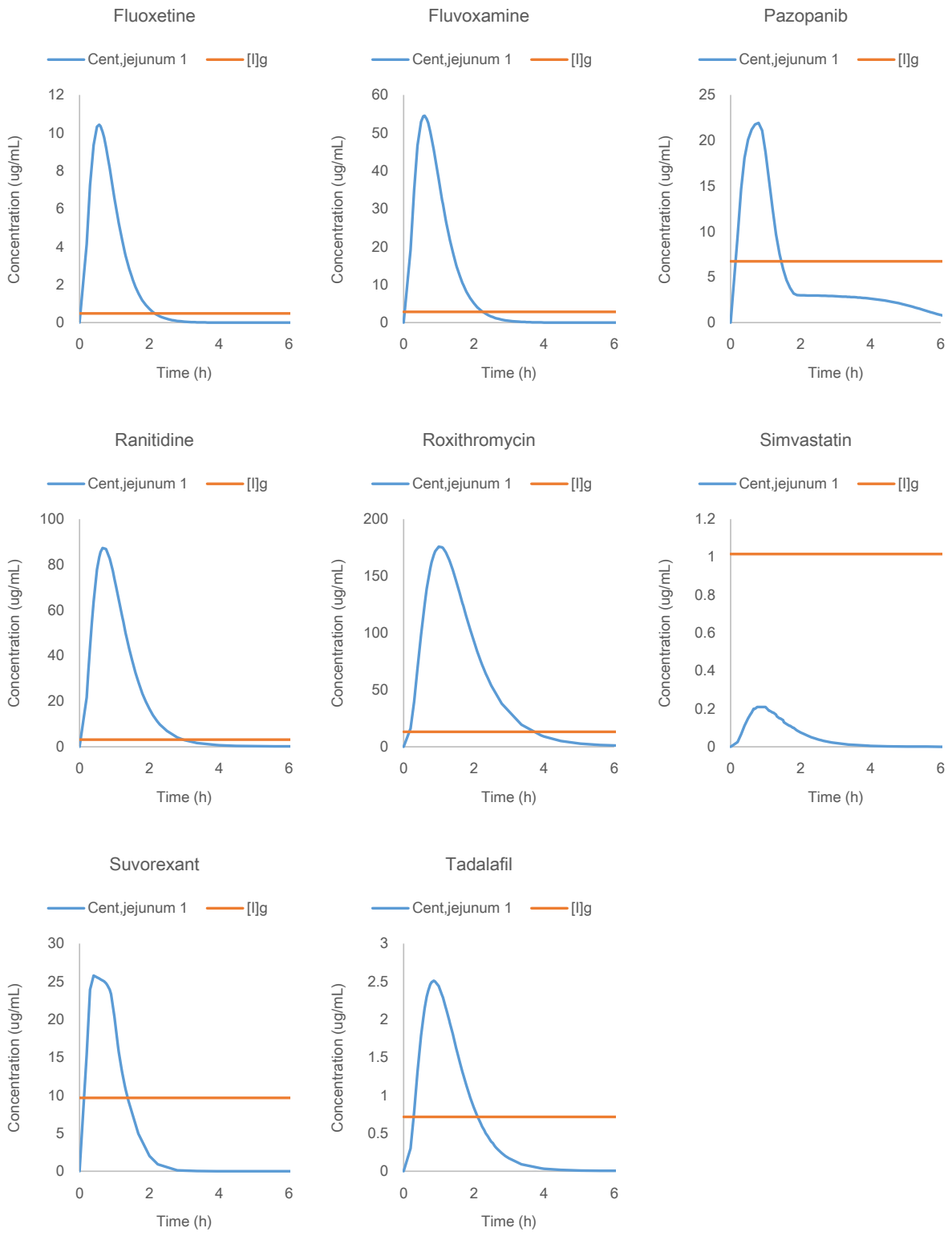
Fluoxetine
Cent,jejunum 1
[I]g
Concentration (ug/mL)
Time (h)
Fluvoxamine
Cent,jejunum 1
[I]g
Concentration (ug/mL)
Time (h)
Pazopanib
Cent,jejunum 1
[I]g
Concentration (ug/mL)
Time (h)
Ranitidine
Cent,jejunum 1
[I]g
Concentration (ug/mL)
Time (h)
Roxithromycin
Cent,jejunum 1
[I]g
Concentration (ug/mL)
Time (h)
Simvastatin
Cent,jejunum 1
[I]g
Concentration (ug/mL)
Time (h)
Suvorexant
Cent,jejunum 1
[I]g
Concentration (ug/mL)
Time (h)
Tadalafil
Cent,jejunum 1
[I]g
Concentration (ug/mL)
Time (h)

Supplemental Figure 6 Comparison of predicted AUCR of midazolam using GastroPlus and static model in the liver for CYP3A inhibition (A) and induction (B).

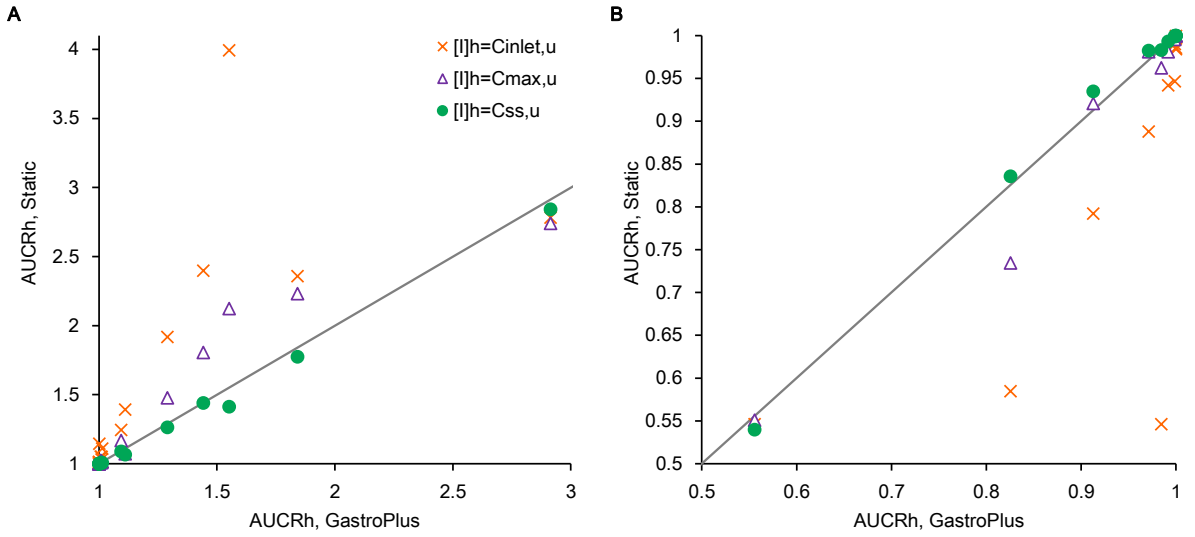

The maximum unbound plasma concentration at the inlet to the liver ($C_{inlet,u}$), maximal unbound plasma concentration ($C_{max,u}$), and steady state unbound plasma concentration ($C_{ss,u}$) were used as the concentration of the perpetrator in the liver ($[I]_h$). To calculate $C_{inlet,u}$, the following equation was used:

$Ci_{nlet,u} = f_{u,p} \times (C_{max} + F_a \times k_a \times Dose/Q_h/R_b)$ (Ito *et al.*, 1998)

where $f_{u,p}$ is the unbound fraction in plasma, C_{max} is the maximal total (free and bound) inhibitor concentration in the plasma at steady state, Q_h is the hepatic blood flow (97 L/h/70 kg), (Yang *et al.*, 2007) and R_b is the blood-to-plasma concentration ratio. C_{ss} was calculated by dividing AUC_{inf} by the dosing interval.

When calculating $[I]_h$, AUC_{inf} at single dose and C_{max} at multiple dose (the same conditions as for DDI simulation) were simulated with GastroPlus and used. F_a, k_a, R_b, AUC_{inf}, and C_{max} used for the static model analysis are shown in Supplemental Table 2.

Most compounds showed a very weak potential for inhibition or induction in liver; therefore, only a few compounds can be used for the comparison. When C_{inlet} and $C_{max,u}$ were used for $[I]_h$, the AUCR in the liver by static model was larger than that by GastroPlus, and when $C_{ss,u}$ was used, they were comparable (Supplemental Figure 3A). For DDI via induction, the predicted effect was larger by static models than that by GastroPlus when C_{inlet} and $C_{max,u}$ were used, and was comparable when $C_{ss,u}$ was used (Supplemental Figure 3B).

Supplemental Figure 7 Concentrations in the liver simulated by GastroPlus ($C_{liver,u}$) and calculated for static model ($C_{inlet,u}$, $C_{max,u}$, and $C_{ss,u}$).

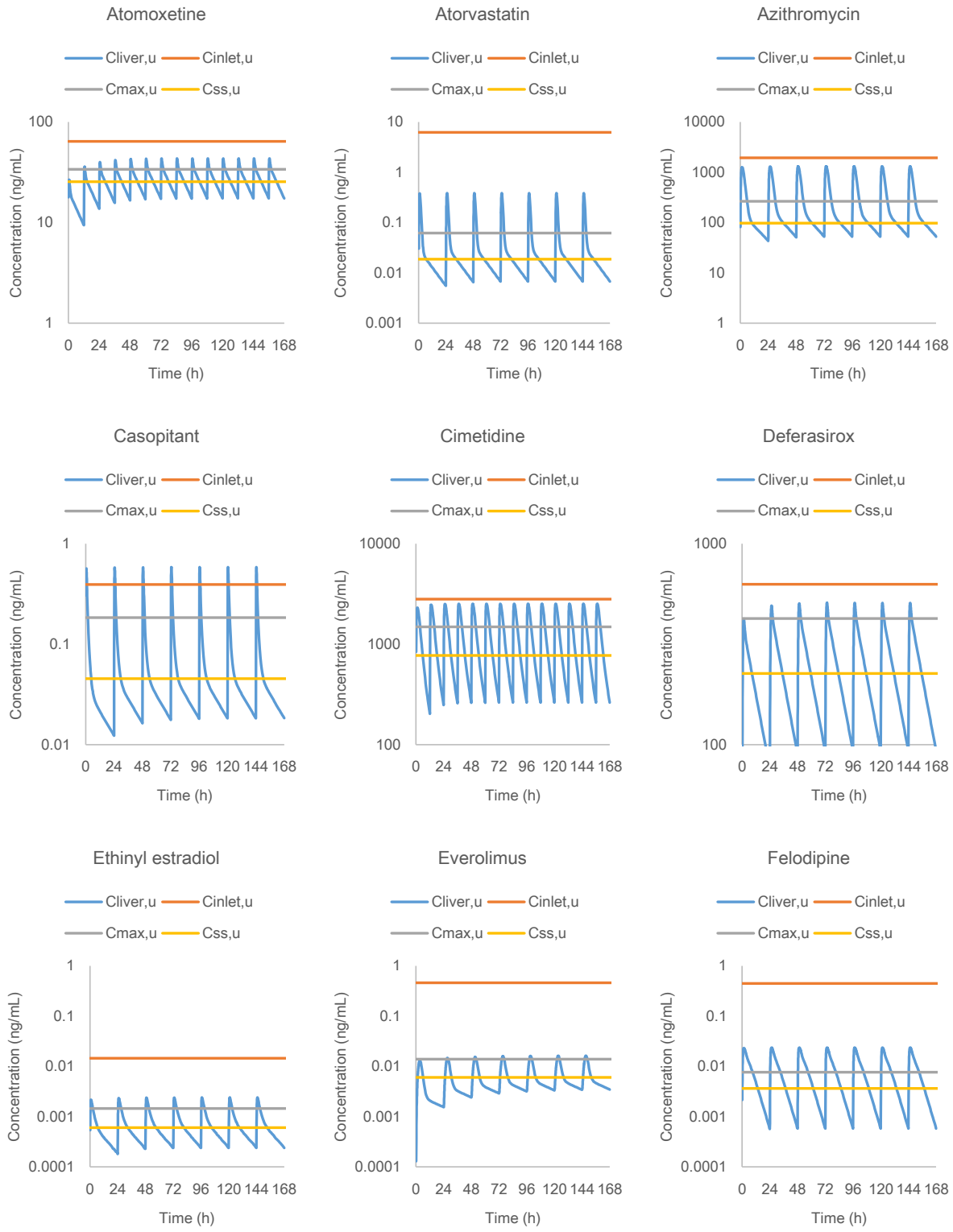

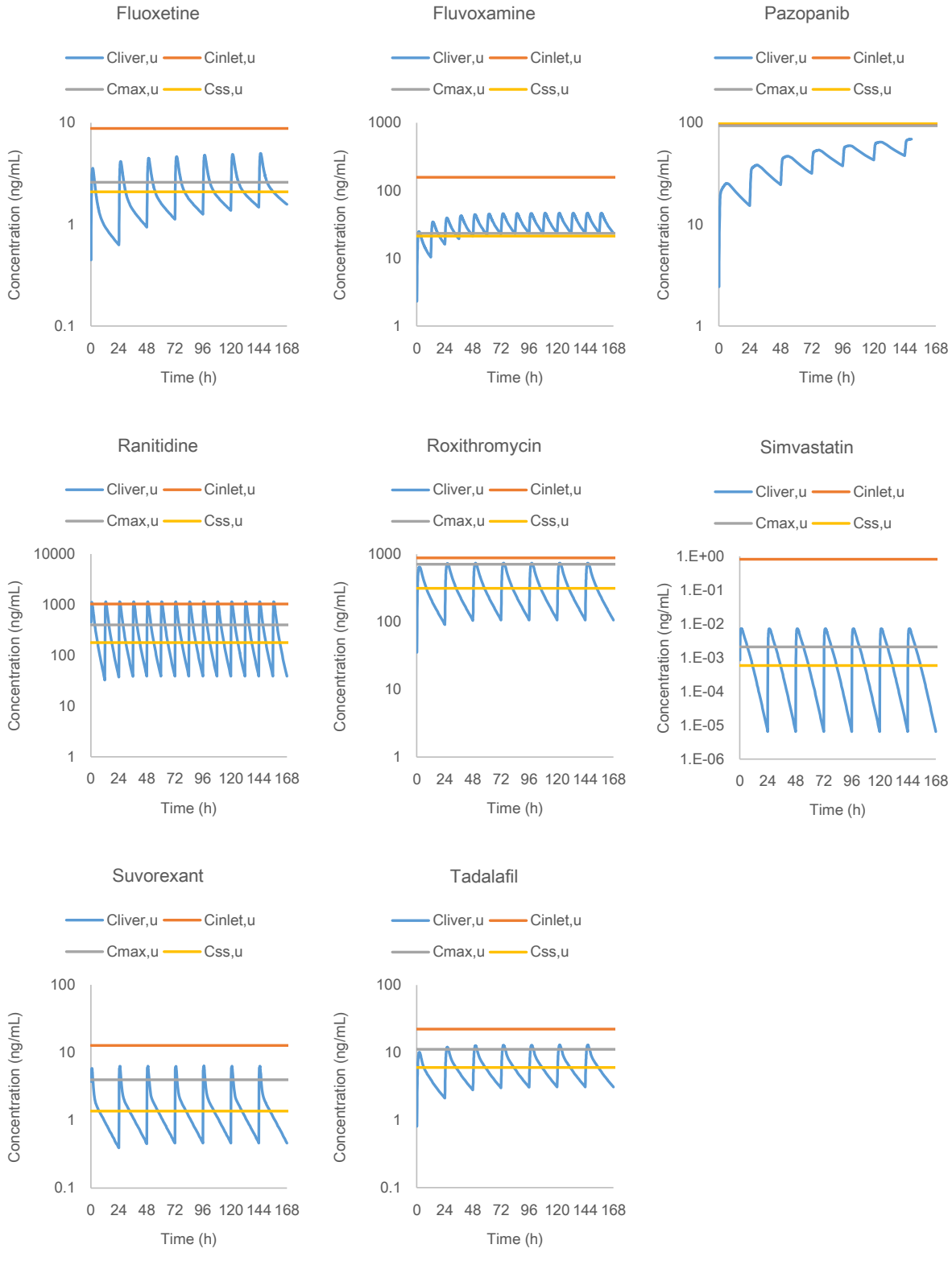
Fluoxetine
Fluvoxamine
Pazopanib
Ranitidine
Roxithromycin
Simvastatin
Suvorexant
Tadalafil
Cliver,u
Cinlet,u
Cmax,u
Css,u
Concentration (ng/mL)
Time (h)
0 24 48 72 96 120 144 168

Supplemental Reference

Albaugh DR, Fullenwider CL, Fisher MB, and Hutzler JM (2012) Time-dependent inhibition and estimation of CYP3A clinical pharmacokinetic drug-drug interactions using plated human cell systems. *Drug Metab Dispos* **40**:1336–1344.

Backman JT, Aranko K, Himberg JJ, and Olkkola KT (1994) A pharmacokinetic interaction between roxithromycin and midazolam. *Eur J Clin Pharmacol* **46**:551–555.

Belle DJ, Callaghan JT, Gorski JC, Maya JF, Mousa O, Wrighton SA, and Hall SD (2002) The effects of an oral contraceptive containing ethinyloestradiol and norgestrel on CYP3A activity. *Br J Clin Pharmacol* **53**:67–74.

Biradar S V., Patil AR, Sudarsan G V., and Pokharkar VB (2006) A comparative study of approaches used to improve solubility of roxithromycin. *Powder Technol* **169**:22–32.

Chang SY, Chen C, Yang Z, and Rodrigues AD (2009) Further assessment of 17alpha-ethinyl estradiol as an inhibitor of different human cytochrome P450 forms in vitro. *Drug Metab Dispos* **37**:1667–1675.

Chantot J, Bryskier A, and Gasc J (1986) Antibacterial activity of roxithromycin: a laboratory evaluation. *J Antibiot* **39**:660–668.

Cook JA, Randinitis EJ, Bramson CR, and Wesche DL (2006) Lack of a pharmacokinetic interaction between azithromycin and chloroquine. *Am J Trop Med Hyg* **74**:407–412.

Cui D, Cabalu T, Yee KL, Small J, Li X, Liu B, Maciolek C, Smith S, Liu W, McCrea JB, and Prueksaritanont T (2016) In vitro and in vivo characterisation of the metabolism and disposition of suvorexant in humans. *Xenobiotica* **46**:882–895.

Edgar B, Lundborg P, and Regårdh CG (1987) Clinical Pharmacokinetics of Felodipine. *Drugs* **34 Suppl 3**:16–27.

Fahmi OA, Maurer TS, Kish M, Cardenas E, Boldt S, and Nettleton D (2008) A combined model for predicting CYP3A4 clinical net drug-drug interaction based on CYP3A4 inhibition, inactivation, and induction determined in vitro. *Drug Metab Dispos* **36**:1698–1708.

Fee JPH, Collier PS, Howard PJ, and Dundee JW (1987) Cimetidine and ranitidine increase midazolam bioavailability. *Clin Pharmacol Ther* **41**:80–84.

Fleishaker JC, and Hulst LK (1994) A pharmacokinetic and pharmacodynamic evaluation of the combined administration of alprazolam and fluvoxamine. *Eur J Clin Pharmacol* **46**:35–39.

Foti RS, Rock DA, Wienkers LC, and Wahlstrom JL (2010) Selection of alternative CYP3A4 probe substrates for clinical drug interaction studies using in vitro data and in vivo simulation. *Drug Metab Dispos* **38**:981–987.

Gascon MP, and Dayer P (1991) In vitro forecasting of drugs which may interfere with the biotransformation of midazolam. *Eur J Clin Pharmacol* **41**:573–578.

Goh BC, Reddy NJ, Dandamudi UB, Laubscher KH, Peckham T, Hodge JP, Suttle AB, Arumugham T, Xu Y, Xu

CF, Lager J, Dar MM, and Lewis LD (2010) An evaluation of the drug interaction potential of pazopanib, an oral vascular endothelial growth factor receptor tyrosine kinase inhibitor, using a modified cooperstown 5+1 cocktail in patients with advanced solid tumors. *Clin Pharmacol Ther* **88**:652–659.

Hang TJ, Zhang M, Song M, Shen JP, and Zhang YD (2007) Simultaneous determination and pharmacokinetic study of roxithromycin and ambroxol hydrochloride in human plasma by LC-MS/MS. *Clin Chim Acta* **382**:20–24.

Heath EI, Forman K, Malburg L, Gainer S, Suttle AB, Adams L, Ball H, and LoRusso P (2012) A phase I pharmacokinetic and safety evaluation of oral pazopanib dosing administered as crushed tablet or oral suspension in patients with advanced solid tumors. *Invest New Drugs* **30**:1566–1574.

Ito K, Iwatsubo T, Kanamitsu S, Ueda K, Suzuki H, and Sugiyama Y (1998) Prediction of pharmacokinetic alterations caused by drug-drug interactions: metabolic interaction in the liver. *Pharmacol Rev* **50**:387–412.

Kenny JR, Mukadam S, Zhang C, Tay S, Collins C, Galetin A, and Khojasteh SC (2012) Drug-drug interaction potential of marketed oncology drugs: In vitro assessment of time-dependent cytochrome P450 inhibition, reactive metabolite formation and drug-drug interaction prediction. *Pharm Res* **29**:1960–1976.

Kokudai M, Inui N, Takeuchi K, Sakaeda T, Kagawa Y, and Watanabe H (2009) Effects of statins on the pharmacokinetics of midazolam in healthy volunteers. *J Clin Pharmacol* **49**:568–573.

Kwon JW, and Armbrust KL (2008) Aqueous solubility, n-octanol-water partition coefficient, and sorption of five selective serotonin reuptake inhibitors to sediments and soils. *Bull Environ Contam Toxicol* **81**:128–135.

Lam YWF, Alfaro CL, Ereshefsky L, and Miller M (2003) Pharmacokinetic and Pharmacodynamic Interactions of Oral Midazolam with Ketoconazole, Fluoxetine, Fluvoxamine, and Nefazodone. *J Clin Pharmacol* **43**:1274–1282.

Mao J, Tay S, Khojasteh CS, Chen Y, Hop CE, and Kenny JR (2016) Evaluation of time dependent inhibition assays for marketed oncology drugs: comparison of human hepatocytes and liver microsomes in the presence and absence of human plasma. *Pharm Res* **33**:1204–1219.

Marshall WL, Feng HP, Caro L, Talaty J, Guo Z, Huang X, Panebianco D, Ma J, Mangin E, O'Reilly TE, Butterton JR, and Yeh WW (2017) No clinically meaningful pharmacokinetic interaction between the hepatitis C virus inhibitors elbasvir and grazoprevir and the oral contraceptives ethinyl estradiol and levonorgestrel. *Eur J Clin Pharmacol* **73**:593–600.

Mc Donnell CG, Shorten G, and Van Pelt FN (2005) Effect of atorvastatin and fluvastatin on the metabolism of midazolam by cytochrome P450 in vitro. *Anaesthesia* **60**:747–753.

Motta P, Pons N, Pagliarusco S, Pellegatti M, and Bonomo F (2011) Casopitant: in vitro data and SimCyp simulation to predict in vivo metabolic interactions involving cytochrome P450 3A4. *Drug Metab Dispos* **39**:363–372.

Obach RS, Walsky RL, Venkatakrishnan K, Gaman EA, Houston JB, and Tremaine LM (2006) The utility of in vitro

cytochrome P450 inhibition data in the prediction of drug-drug interactions. *J Pharmacol Exp Ther* **316**:336–348.

Pellegatti M, Bordini E, Fizzotti P, Roberts A, and Johnson BM (2009) Disposition and metabolism of radiolabeled casopitant in humans. *Drug Metab Dispos* **37**:1635–1645.

Peveling-Oberhag J, Zeuzem S, Yong WP, Kunz T, Paquet T, Bouillaud E, Urva S, Anak O, Sellami D, and Kobalava Z (2013) Effects of Hepatic Impairment on the Pharmacokinetics of Everolimus: A Single-Dose, Open-Label, Parallel-Group Study. *Clin Ther* **35**:215–225.

Ring BJ, Patterson BE, Mitchell MI, Vandenbranden M, Gillespie J, Bedding AW, Jewell H, Payne CD, Forgue ST, Eckstein J, Wrighton SA, and Phillips DL (2005) Effect of tadalafil on cytochrome P450 3A4-mediated clearance: Studies in vitro and in vivo. *Clin Pharmacol Ther* **77**:63–75.

Rowland Yeo K, Walsky RL, Jamei M, Rostami-Hodjegan A, and Tucker GT (2011) Prediction of time-dependent CYP3A4 drug-drug interactions by physiologically based pharmacokinetic modelling: Impact of inactivation parameters and enzyme turnover. *Eur J Pharm Sci* **43**:160–173.

Sauer JM, Long AJ, Ring B, Gillespie JS, Sanburn NP, DeSante KA, Petullo D, VandenBranden MR, Jensen CB, Wrighton SA, Smith BP, Read HA, and Witcher JW (2004) Atomoxetine hydrochloride: clinical drug-drug interaction prediction and outcome. *J Pharmacol Exp Ther* **308**:410–418.

Serajuddin AT, Ranadive SA, and Mahoney EM (1991) Relative lipophilicities, solubilities, and structure‐pharmacological considerations of 3‐hydroxy‐3‐methylglutaryl‐coenzyme A (HMG‐CoA) reductase inhibitors pravastatin, lovastatin, mevastatin, and simvastatin. *J Pharm Sci* **80**:830–834.

Skerjanec A, Wang J, Maren K, and Rojkjaer L (2010) Investigation of the pharmacokinetic interactions of deferasirox, a once-daily oral iron chelator, with midazolam, rifampin, and repaglinide in healthy volunteers. *J Clin Pharmacol* **50**:205–213.

Snyder BD, Rowland A, Polasek TM, Miners JO, and Doogue MP (2014) Evaluation of felodipine as a potential perpetrator of pharmacokinetic drug-drug interactions. *Eur J Clin Pharmacol* **70**:1115–1122.

Tiseo PJ, Perdomo CA, and Friedhoff LT (1998) Concurrent administration of donepezil HCl and cimetidine: assessment of pharmacokinetic changes following single and multiple doses. *Br J Clin Pharmacol* **46 Suppl 1**:25–29.

Todor I, Popa A, Neag M, Muntean D, Bocsan C, Buzoianu A, Vlase L, Gheldiu AM, and Briciu C (2016) Evaluation of a potential metabolism-mediated drug-drug interaction between atomoxetine and bupropion in healthy volunteers. *J Pharm Pharm Sci* **19**:198–207.

Urva S, Bouillaud E, Delaney R, Jappe A, and Cheung W (2013) A phase I study evaluating the effect of everolimus on the pharmacokinetics of midazolam in healthy subjects. *J Clin Pharmacol* **53**:444–450.

van Crugten J, Bochner F, Keal J, and Somogyi A (1986) Selectivity of the cimetidine-induced alterations in the renal handling of organic substrates in humans. Studies with anionic, cationic and zwitterionic drugs. *J Pharmacol Exp Ther* **236**:481–487.

von Moltke LL, Greenblatt DJ, Schmider J, Duan SX, Wright CE, Harmatz JS, and Shader RI (1996) Midazolam hydroxylation by human liver microsomes in vitro: inhibition by fluoxetine, norfluoxetine, and by azole antifungal agents. *J Clin Pharmacol* **36**:783–791.

Wu K, Xu J, Fong R, Yao X, Xu Y, Guiney W, Gray F, and Lockhart A (2016) Evaluation of the safety, pharmacokinetics, pharmacodynamics, and drug-drug interaction potential of a selective Lp-PLA2 inhibitor (GSK2647544) in healthy volunteers. *Int J Clin Pharmacol Ther* **54**:935–949.

Yamazaki T, Desai A, Goldwater R, Han D, Lasseter KC, Howieson C, Akhtar S, Kowalski D, Lademacher C, Rammelsberg D, and Townsend R (2017) Pharmacokinetic Interactions Between Isavuconazole and the Drug Transporter Substrates Atorvastatin, Digoxin, Metformin, and Methotrexate in Healthy Subjects. *Clin Pharmacol Drug Dev* **6**:66–75.

Yang J, Jamei M, Yeo KR, Rostami-Hodjegan A, and Tucker GT (2007) Misuse of the well-stirred model of hepatic drug clearance. *Drug Metab Dispos* **35**:501–502.

Yeates RA, Laufen H, and Zimmermann T (1996) Interaction between midazolam and clarithromycin: comparison with azithromycin. *Int J Clin Pharmacol Ther* **34**:400–405.

Zamuner S, Johnson BM, Pagliarusco S, Fina P, Peroni M, Fiore M, Adams LM, and Fernandes SA (2010) Effect of single and repeat doses of casopitant on the pharmacokinetics of CYP450 3A4 substrates midazolam and nifedipine. *Br J Clin Pharmacol* **70**:537–546.

Zhi J, Moore R, Kanitra L, and Mulligan TE (2003) Effects of orlistat, a lipase inhibitor, on the pharmacokinetics of three highly lipophilic drugs (amiodarone, fluoxetine, and simvastatin) in healthy volunteers. *J Clin Pharmacol* **43**:428–435.

Zimmerlin A, Trunzer M, and Faller B (2011) CYP3A time-dependent inhibition risk assessment validated with 400 reference drugs. *Drug Metab Dispos* **39**:1039–1046.